CYPRUS UNIVERSITY OF TECHNOLOGY

DEPARTMENT OF CIVIL ENGINEERING AND GEOMATICS

Postgraduate Thesis

MONITORING WATER QUALITY CHARACTERISTICS OVER ASPROKREMMOS AND KOURRIS DAMS USING REMOTE SENSING

Anastasios Giannakou

Limassol, September 2016

CYPRUS UNIVERSITY OF TECHNOLOGY

FACULTY OF ENGINEERING AND TECHNOLOGY

DEPARTMENT OF CIVIL ENGINEERING AND GEOMATICS

MONITORING WATER QUALITY CHARACTERISTICS OVER ASPROKREMMOS AND KOURRIS DAMS USING REMOTE SENSING

by

Anastasios Giannakou

Limassol, September 2016

APPROVAL FORM

Postgraduate Thesis

MONITORING WATER QUALITY CHARACTERISTICS OVER ASPROKREMMOS AND KOURRIS DAMS USING REMOTE SENSING

Presented by

Anastasios Giannakou

Dissertation Supervisor: Professor Diofantos Hadjimitsis

Signature_____

Committee member:

Signature_____

Committee member

Signature_____

Cyprus University of Technology

September 2016

Intellectual rights

Copyright © Anastasios Giannakou, 2016

All rights reserved.

The approval of the thesis from the Department of Civil Engineering and Geomatics of the Cyprus University of Technology does not necessarily imply acceptance of the opinions of the author, on behalf of the Department.

I would like to thank Professor Diofantos Hadjimitsis for his useful supervisory guidance. To Dr Christiana Papoutsa along with Mr Demetris Kouhartsiouk, both research fellows of Cyprus University of Technology, who provided me with useful research information and detailed guidance for the operation of ENVI 4.8 software package, and for that I owe them my appreciation.

I dedicate this project to my dearest Uncle, Sotiris Giannakou, who passed away recently of cancer. I would also like to dedicate this study to my mother and father, Androulla Siampetta and Andreas Giannakou, who also suffer incurable diseases such as Motor Neuron Disease and Lung Cancer, respectively.

I would like to give my special thanks to Antri Georgiou who stood by my every step of the way.

Data available from the U.S. Geological Survey.

Abstract

Remote sensing techniques were utilised in order to investigate water quality parameters of the two largest dams located in Cyprus, Asprokremmos and Kourris. Recent studies showed that dams were classified as oligotrophic to mesotrophic states but only concerned classification for a short period of time. In this study, a ten year approach from 2006 until present was conducted for both dams in order to examine their overall behaviour in terms of Chlorophyll-a (Chl-a) and Turbidity concentrations values and thereafter to their correlation with Trophic State Index (TSI).

In total, ten digital images from Landsat 5 Thematic Mapper (TM) and five from Landsat 8 Operational Land Imager (OLI) were acquired from United States Geological Survey (USGS) concerning the abovementioned time of period.

For the pre-processing of all digital images, radiometric and atmospheric correction was performed to obtain reflectance values. It was observed that dams of Asprokremmos and Kourris indicated rational water reflectance values for all the selected bands, Red-Green-Blue (RGB), and where it was possible, validation was done utilising in-situ spectral signatures. Otherwise, findings were compared with other studies reflectance's outputs. Furthermore, four algorithms were applied to retrieve water quality parameters as the post-processed part of this study. The turbidity and TSI algorithms which were originally developed for Asprokremmos dam and Landsat 5 TM, was also tested for Kourris dam and Landsat 8 OLI. For Chl-a concentrations, two proposed algorithms were found in literature concerning the two satellites bands' characteristics and other study areas were also tested.

From the final results, it was concluded that the turbidity algorithm performed well at Kourris dam. For Asprokremmos dam, the estimated turbidity mean values data showed similar findings with empirical in-situ data collected from past campaigns. Chl-a algorithms also presented rational concentrations at both dams but it was assumed that due to no calibration, final results may be questioned, especially for Kourris dam. Linear regression models were created weighting differently for each parameter and dam and a correlation with the estimated TSI values was achieved scoring up to 0.59 for Asprokremmos and 0.37 for Kouris. Low values of correlation were justified by the fact that the time periods among the acquisition dates been examined where not always even and thereafter influenced the overall variation of the parameters' mean values.

Table of Contents

Table of Tables

Table of Figures

Abbreviations

ASTER	Advanced Spaceborne Thermal Emission and Reflection Radiometer
CDOM	Coloured Dissolved Organic Matter
Chl-a	Chlorophyll-a
ESA	European Space Agency
FLAASH	Fast Line-of-Sight Atmospheric Analysis of Spectral Hypercubes
GOGI	Geostationary Ocean Color Imager
Landsat 5 TM	Landsat 5 Thematic Mapper
Landsat 7 ETM+	Landsat 7 Enhanced Thematic Mapper Plus
Landsat 8 OLI	Landsat 8 Operational Land Imager
MERIS	MEdium Resolution Imaging Spectrometer
MODTRAN	MODerate resolution TRANsmission code
NASA	National Aeronautics and Space Administration
OCLI	Ocean Land Colour Instrument
RMSE	Root Mean Square Error
SDT	Secchi-Disk Trasparency
TOA	Top of the Atmosphere
TP	Total Phosphorus
TSI	Trophic State Index
USGS	United States Geological Survey

1 Introduction

1.1 Introductory remarks

Water is a vital natural resource for humanity and ecosystem health, confronts various pollution risks that result to the deterioration of its overall quality. The major cause of this phenomenon is mainly human activities such as industrial effluents, agricultural waste and sewage treatment which end by river streaming into lakes and dams (Usali & Ismail, 2010, p. 228). More specifically, water quality parameters such as Chlorophyll-a (Chl-a) and turbidity are the most common factors which contribute extensively to the contamination of water resources.

The European Union, as one of the largest environment protectors, was able to achieve to introduce nationally the European Water Framework Directive in 2000 as a countermeasure against further pollution of the water resources. The main goal of this directive is the protection and improvement of aquatic ecosystems including oceanic and inland water by the avoidance or reduction of the water deterioration caused by human activities. In total, 25 laws had being introduced for the purpose of monitoring and assessing water bodies by the member states (Schaber-Schoor, 2010).

Nowadays, current practices for the purpose of assessment and monitoring of water bodies' quality parameters are mainly two, in-situ inspections and the utilisation of remote sensing technologies. The first can be described as a method that obtains accurate and detailed information describing the real behaviour of a water body only with a disadvantage of being time and cost consuming. The latter, is the utilisation of aerospace devices such as satellites which can effectively reduce the economic aspects of the major problem. In particular, satellites are state of the art technological equipment that is capable to synoptically cover the globe. They are consisted by a wide range of instruments and they have the potential of filling the gap of missing in-situ data and provided data in a systematic basis. Their drawback is that the data retrieved from their sensors are just an estimation of the water parameters only for the top surface of the water body being examined.

1.2 Project Purpose

The aim of this research was the collection and examination of water quality parameters for the two biggest water reservoirs in Cyprus, Asprokremmos and Kourris dams, by utilising existing satellite data from the past ten years, 2006 to 2016. Results obtained from post-processing of the selected satellite images primarily indicated for both water bodies their trophic states indexes and secondary the correlation of Chla-a with turbidity.

Furthermore, the examination of the two dams at the aforementioned time period was also expected to signify various water quality parameters' patterns mostly caused when the dams were either near empty, moderated or filled with water. This will enable a better understanding of both dams' behaviour over seasonal and yearly alterations due to droughts or overflow and how its morphology and their main supply rivers can affect their overall quality.

The major benefit of this study is the evaluation of both dams' water quality characteristics mostly pointing past incidences and the future uprising problems caused from Chl-a and turbidity in terms of their environmental impact. In addition, this study can also benefit civil engineers as dams are manmade structures and water quality conservation is one of primary goals that must be taken into consideration when construction of these kinds of infrastructures occurs.

2 Literature review

2.1 Introduction

The following chapter aims to present and examine various factors that may influence water quality in inland water bodies. Various techniques are also mentioned in this chapter describing procedures needed to be applied for systematic monitoring of water quality parameters such as Chl-a and turbidity.

2.2 Water Quality Parameters

2.2.1 Chlorophyll-a

Chl-a can be described as living organism which develops mainly in inland and coastal waters. Development of this organism totally depends on the concentration of nutrients phosphorus, nitrogen and the sunlight being received in a certain time period. Mostly, Chl-a can be detected by its distinctive light green colour covering the surface water of a reservoir or a river.

Figure 2.1: Green algae (chlorophyll-a) on British canals and lakes.

Phosphorus and other nutrients can be found in water bodies by either physical or manmade aspects. Sources that are considered as non-points such as river water in combination with ground water absorb and transport nutrients from agricultural or physical processes of landscapes with final destination the inland water bodies. Point sources such as industrial areas, pipes or ditches also pollute and reach water bodies with similar ways. Depending of

the weather conditions and the amount of sunlight that passes water, Chl-a is developed accordingly (Ritchie, Zimba & Everitt, 2003, p.695). Consequently, the water quality characteristics of inland water bodies such as lakes and dams are drastically altered by affecting biodiversity and their use. According to their study, alteration of water quality characteristics affects quality standards for water used for human consumption. That actually implies to the deterioration of the water's physical, chemical, and biological parameters. Additionally, due to the fact that in situ measurements are time consuming in terms of economy and procedures, constant monitoring cannot be sustained for long time of periods. Therefore, valuable information regarding water's quality parameters might be lost during time overlapping.

2.2.2 Turbidity

Along with chl-a, turbidity also coexists in large water bodies. Turbidity can be simply explained as dissolved organic matter being suspended in the water. Different substances formed in water or large particles introduced from exogenous parameters are contained in water bodies deteriorating its quality. Turbidity can be distinguished by the light grey colour and when in situ measurements occur, objects are not visible after a certain depth.

Main sources of turbidity derives especially by clay and silt, fine organic and inorganic matter, soluble coloured organic compounds, algae and other microscopic organisms. Physical sources that create this parameter are erosion form upland and stream channel areas. Manmade sources often accelerate this erosion by the introduction of acids in the streams or phosphorus being washed in the waters by the wastewater treatment facilities (Minnesota Pollution Control Agency, 2008, p.1).

In addition, in the last decade it was observed that turbidity influence lakes' thermal patterns. As a variety of particles are included in the body of water and considering that the amount of their concentrations defects water quality, subsequently the water body's chemical and biological parameters are altered. This can lead to a rapid change of the water surface temperature and, in a further stage, the water-atmosphere transfer (Potes, Costa & Salgado, 2012, p. 1623).

Figure 2.2: Shows turbidity being washed from river to ocean.

2.2.3 Sechhi-disk Transparency

Secchi-disk is one of the most common used tools in order to estimate empirically the turbidity of water. It is a circular dimensioned object, colored with black and white quadrants attached to measuring tape. The instrument is lowered into the water and measurements are taken when there is a condition of invisibility due to turbid waters.

A massive drawback of Secchi disk is that there are no standardisation models to be introduced for its manufacturing properties. In previous years, different Secchi disks were produced with no standard size and colour intensity which in some cases the accuracy was unclear concerning the visibility that varied because of the size of the disk. Another important parameters influencing Secchi disk accuracy are the disk image dissection by surface refraction of the light path, boat's shadow and the sun's position when measurements are taken (Smith & Hoover, 2000, p.2).

Standard procedures for obtaining Secchi disk measurements clearly points that in order to avoid undesirable errors, measurements shall be taken in the shaded side of the boat where reflection will not be involved. Moreover, it is advised that when currents cause the disk to drift, added weight must be included in order to minimise skewed measurements (RIDEM - Office of Water Resources, 2011, p.4).

2.2.4 Trophic State Index

During overflow seasons, a variety of nutrients such as nitrogen and phosphorus are added into water bodies contributing to the development of chl-a. In the same way, suspended and organic matter immigrates and concentrates creating biomass which in the end deteriorates the overall health of the water body. Depending on the concentrations of the aforementioned parameters, trophic states can be categorised indicating the current pollution of the water body (Stednick & Hall, p.2).

To estimate and evaluate the health of a water body, four categories of eutrophication were created in order describe the level of pollution. The amount of concentration of nutrients, Chl-a and turbidity in inland water bodies can be classified into four categories (Fuller & Jodoin, 2016, p.2):

1. Oligotrophic where the concentrations of nutrients, Chl-a and turbidity are minimal,
2. Mesotrophic where moderate concentrations are present,
3. Eutrophic and,
4. Hypertrophic where maximal concentrations indicate that the water body is in high levels of pollution.

The most common evaluation model which is Carlson's Trophic State Index (TSI), depends on three variables. Chl-a, Seechi disk depth and Total Phosphorus (TP) are numerically determined in order to evaluate and assess the eutrophication of water bodies (Prasad & Siddaraju, 2012, p.2992). The table below shows the average values for Oligotrophic, Mesotrophic, Eutrophic and Hypertrophic states.

Table 2.1: Shows the average values for Trophic State Index (TSI), Secchi-disk Trasparency (SDT), Total Phosphorus (TP) and Chlorophyll-a.

Lake Trophic Condition	TSI Value	SDT (m)	Chl-a (µg/L)	TP (µg/L)
Oligotrophic	<30 - 40	4 - 8<	0 - 2.6	0 - 12
Mesotrophic	40 - 50	2 - 4	2.6 –20	12 - 24
Eutrophic	50 - 70	0.5 – 2	20 - 56	24 - 96
Hypertrophic	70 - 100+	0.5 - 0.25>	56 – 155+	96 – 384+

Source: Fuller & Jodoin, 2016, p. 2.

2.3 Practises for Monitoring Water Quality Parameters

2.3.1 In-situ

As mention in previous subsectors, one of the main procedures that are followed for water quality assessment is in-situ inspections and measurements. Laboratory testing for each sample is performed and concentrations of mainly Chl-a, TP and suspended matter can be retrieved accurately. The main drawback of this procedure is that sampling concerns only certain geographical location and depth measurements in the water. Therefore, in order to estimate the average behaviour of the water, sampling can be numerous and time consuming. Consequently, different approach is required each time as water bodies differ in morphology and chemical composition. For example, if there are two input rivers which end in a lake, high turbid water will be mostly seen at the rivers resting expanding to the very end of the lake due to water movement.

Another example which only concerns Chl-a pollution patterns, is when stagnant water is present. This allows organism to develop more easily and in some cases, Chl-a growth expands to highly dangerous levels. Nevertheless, in-situ measurements are substantial as they are mostly used for validation purposes when satellite technologies are applied.

2.3.2 Spectral Signatures

Spectral signature is a characteristic of materials to reflect a percentage of energy emitted by the sun. Each material can absorb energy in a different way in all wavebands, thus the utilisation of spectral signatures becomes important when extracting information from satellite images (Aggarwal, n.d., p.32). The principle behind spectral signatures is the overall reflectance being retrieved by spectrometers which either are used in field or in satellites. The equation bellow describes the reflectance:

For reflectance λ: $$\Phi(\lambda) = r_\lambda + \tau_\lambda + a_\lambda \text{ in } W\mu m^{-1} \quad (2.1)$$

Where r_λ is the reflected radiation, τ_λ is the transmitted radiation and a_λ is the absorbed radiation.

For example, clear water as a transparent liquid absorbs the most of the energy mostly depending to the variability of depth, therefore is expected to retrieve the lowest reflectance in the visible range of wavelengths, Blue, Green and Red. Turbid water produces a higher

reflectance depending on the concentration of particles in the water body. Particles scatter the energy and the light does not penetrate to its whole depth. In contrast, vegetation spectral signature differs as in the visible range of wavelength fluctuates at low reflectance due to chlorophyll and at Near Infrared increases dramatically as chlorophyll does not absorb at this range of wavelength.

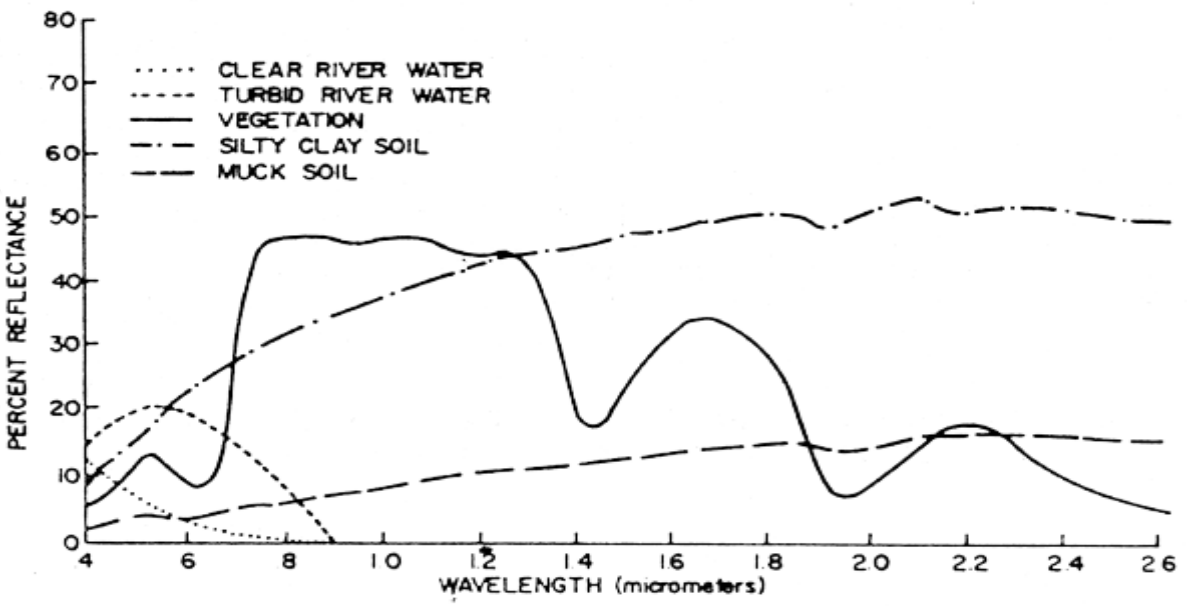

Figure 2.3: Indicates different spectral signatures of water, vegetation and soil.
Source: Food and Agriculture Organisation of the United Nations, n.d.

To obtain excellent quality spectral signatures, field spectroradiometer is utilised. Similar equipment is utilised at satellites for the purpose of identifying various materials from satellite images. The difference with satellite spectroradiometers is that the gap between ground elevation and the altitude of satellite's position, involves atmosphere's aerosols, humidity, clouds, sun altitude and position etc. which at the end deteriorates the quality of results of the reflectance (Papoutsa, 2015, September, pp.1-6).

2.3.3 Satellites & Sensors

Satellites have the capability to detect these parameters easily and in some cases they can retrieve and produce well-presented results just as well as in with situ measurements. The main drawback of utilising satellites is that they utilise empirical approaches to measure any concentration of turbidity or Chl-a. Adding to this, results that are retrieved from satellites can only indicate surface concentrations which at the end it is not representative of the real

behaviour of the examined water body. Nevertheless, the scientific community have succeeded to correlate ground observations with satellite data on a certain level and there is a massive progress in this matter which continuous in the present.

Satellites are equipped with a series of wavelength sensors and according to their capabilities, different information can be retrieved for either land or water studies. Wavelengths that are used from satellites are usually the visible to near infrared and also include wavebands for thermal observation and aerosol retrieval.

More specifically, the multispectral sensors that are used for water quality assessments are the visible wavebands Blue 0.45 to 0.51 μm, Green 0.53 to 0.59 μm, Red 0.64 to 0.67 μm and the non-visible band Near Infrared 0.85 to 0.88 μm (USGS, 2016). For example, retrieval of Chl-a depends on the combination of the two wavebands near infrared divided by the Red (Band 3/Band 1 For Landsat 5). The following table describes the capabilities of each band and what they can be used for.

Table 2.2: Shows the capabilities and characteristics of each band for Satellite Landsat 5 TM.

Band – EMS λ	About
Blue	Penetrates better in clear water but it is absorbed from Chl-a. Therefore, it is difficult to identify plants in this band. Man-made structures are clearly visible.
Green	It has excellent contrast between clear and turbid water. Also detects vegetation. Fairly seen man-made structures.
Red	Can be used to detect vegetation types and soils. Good reflectance of dead foliage but not the same with live foliage with Chl-a.
Near Infrared	Can detect biomass and it is very good to analyse vegetation.

Source: United States Geological Survey (USGS), n.d.

2.3.4 Algorithms & Software

Algorithms are the most vital part of satellites' image processing. They are used after geometric and radiometric calibration, atmospheric correction in order to retrieve Chl-a and turbidity concentrations. In order to perform analysis on satellite images, different types of software in combination with empirical algorithms found in literature are also used as the aforementioned parameters cannot be analysed and detected in a single waveband.

Generally, every satellite's sensors are calibrated to a specific wavelength of the wave spectrum according to their manufacturing purpose. For example, the Advanced Spaceborne Thermal Emission and Reflection Radiometer (ASTER) share the same specifications with

Landsat 5 TM sensors in terms of the visible wavelength spectrum. Specifically, the Green and Red Bands of the both sensors are the same, thus both can be used for the same purpose if it is needed.

In addition, the need of specialised software, e.g. ENVI and ERDAS Imagine, in satellite image processing is crucial as different environments with geographical features and weather conditions are always altered and unique in terms of the time of acquisition. Every analysis will involve different parameters that lead to different results. For instance, a satellite image of an island circled by oceanic water will require different atmospheric correction input parameters than a satellite image with only inland features. The reason is that in the picture on the left require atmospheric correction with input parameters concerning increased water evaporation due to oceanic water. The outcome of results, if the wrong parameters are inputted, the acquired reflectance values will fluctuate in non-logical patterns of describing oceanic water's spectral signature being near to zero percent values, which is not a characteristic of the water.

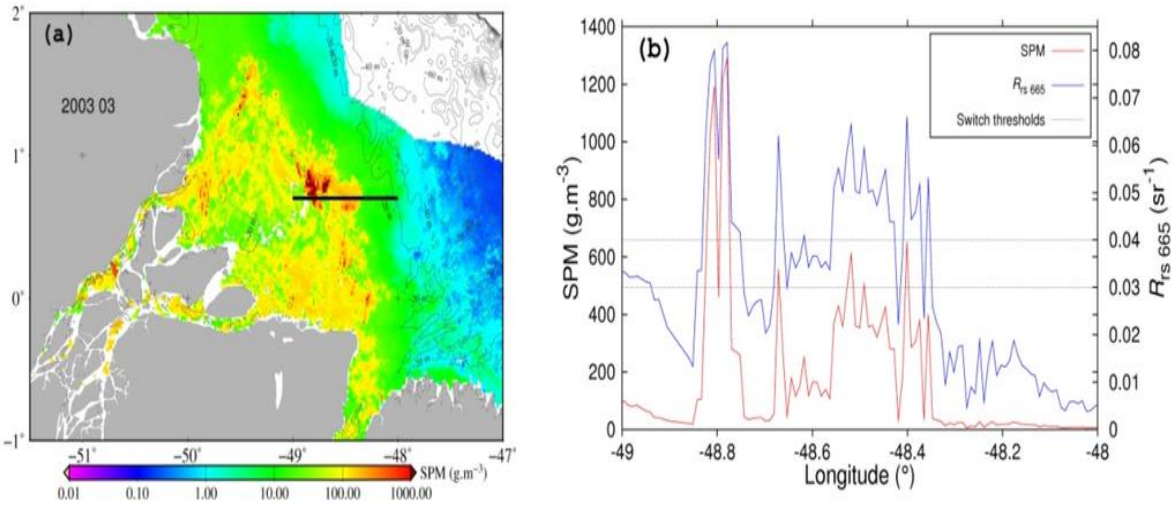

Figure 2.4: An example of a post-processed satellite image indicating turbidity concentrations.
Source: Han et al, 2016, p.16.

2.4 Algorithms for Chlorophyll-a and Turbidity

As mentioned above, algorithms are the most crucial part of satellite image processing. In literature review, a variety of algorithms were proposed for the two parameters Chl-a and Turbidity. To start with, it is worth mentioning that in most cases the final outcomes are primarily the classification of water bodies concerning TSI through the combination of the three parameters of TP, Chl-a and Turbidity concentrations.

For Chl-a, Gilerson et al (2010) suggested that the combination of Red and Near Infrared Bands in order to retrieve Chl-a concentrations, are the most suitable for the case of coastal and inland waters. Their main purpose was to test two-band and three-band algorithms with the utilisation of MEdium Resolution Imaging Spectrometer (MERIS) sensor and validation was performed with the use of in situ datasets obtained from several lakes of Nebraska, United States. They found that both type of algorithms did not totally depend on the absorption properties of coloured dissolved organic matter (CDOM) and other constituents found in water but they were mainly depended on water and phytoplankton absorption coefficients. Furthermore, their findings showed a good correlation between truth and estimated data and they concluded that the specific algorithms can be used without the need of regional calibration.

With the same principle, Augusto-Silva et al (2014, pp.11689-11693), proposed three algorithms in order to investigate Chl-a concentrations in Funil reservoir, Rio de Janeiro, Brazil. The research included in situ measurements for validation purposes, MERIS sensor datasets and as well as Ocean Land Colour Instrument (OCLI) to investigate water quality to the aforementioned reservoir. They explained that the relationship of both Red and Near Infrared Bands minimises the interference of the signal between other components in the water body as they were tested in tropical turbid inland waters. Monte Carlo simulation was also performed for better calibration of the algorithms. Their final concluding remarks were that algorithms performed with 17.85% and 17.64% percentage of errors during the utilisation of MERIS and OCLI data, respectively.

Furthermore, Huang et al (2014, p.38) observed that the number of bands used in algorithms can be crucially deterministic in terms of the retrieving Chl-a concentrations. They studied five major lakes of China with high turbid waters utilising two band and three band algorithms consisted by Near Infrared and Red bands, respectively. Their findings indicated

that the two band algorithm was capable to retrieve low concentrations of Chl-a when extremely turbid waters are presented, and the three band algorithm performed well when with both high turbid water and Chl-a were present. In addition, both algorithms were tested in different models with different sensors, MERIS and Geostationary Ocean Color Imager (GOGI), and a fluctuation of the Root Mean Square Error (RMSE) was observed. This led to the conclusion that the switching of spectral bands to each sensor can alter the final result.

On the other hand, due to the recent launch of Landsat 8 OLI in 2013, there is debate at the scientific community concerning the applicability of the previously validated algorithms. The main concern is that Landsat 5 TM and Landsat 7 Enhanced Thematic Mapper Plus (ETM+) utilised wider bands in the visible range of wavelengths which in some cases can be a drawback if the current satellite is utilised. According to the United States Geographical Survey (2016), significant alteration of the bands' measuring capabilities is found at the Red Band with 0.63 to 0.69 μm for Landsat 5 and 7 and 0.64 to 0.67 μm for Landsat 8 OLI. Consequently, if the validated algorithms used for Landsat 5 TM and 7 ETM+ that were used until now are applied to the current satellite, an increment of error will be included at the final stage of image processing.

In this case, Yang and Anderson (2016, p.134) suggested that with Landsat 8 OLI it is feasible to retrieve Chl-a concentration with the utilisation of Green (B3) and Aerosol (B1) bands as well as Near Infrared (B5) and Green (B3) bands ratios. They utilised two algorithms which were mostly applicable for seasonal purpose, for summer B3/B1 and autumn B5/B3 respectively. Their study was mainly focused in the region of Jordan Lake, the most eutrophic lake at North Carolina, United States. They achieved a good correlation of spectral index between in situ with estimated data despite the fact that limited images were available at the time.

For turbidity, the most used models to retrieve reflectance regarding concentration for this parameter are algorithms with a linear regression models correlated with in situ datasets. According to Papoutsa et al (2013, p. 1687), their research concerned the dam of Asprokremmos in Paphos, Cyprus, where they developed algorithms utilising and testing satellite Landsat 5 TM's bands. They found that the most suitable band for retrieval of turbidity was band 3 (Red) with 90 per cent correlation with in situ datasets acquired during overpasses of the satellite. The correlated results between truth and estimated data showed that the variety of samples collected from the dam as well as reflectance values, fluctuated

from 1 to 25 Nephelometric Turbidity Units (NTU) for turbidity and 0.5% to 6.5% for Band 3 (Red) reflectance values. Furthermore, it was observed that the variety of sampling and reflectance was mainly determined at low values, 1 to 15 NTU and 0.5% to 5%, for turbidity and reflectance values respectively.

Furthermore, Han et al (2016, p. 16) stated that an important factor which influences the accuracy of algorithms for turbidity concentrations are their capability to detect various surface amounts of turbidity concentrations (low, moderated or high concentrations etc.) as well as the area of study of the algorithms being developed for. In their research, they selected various algorithms from literature and they tested them in different coastal environments such as Europe, French Guiana, North Canada, Vietnam and China. The concluded that the controversy regarding the biochemical and physical process that occur at the aforementioned coastal environments, is an important factor to reduce or even contradict the efficiency of the already validated algorithms.

A great example that can be capable to fulfil the abovementioned problem of algorithms, is the utilisation of algorithm regardless the type of water being studied. Dogliotti et al (2015, p. 166) tested an algorithm where they took into consideration more specifically the particles' size but not the type of water, either coastal or estuarine in this case. The algorithm was developed in a way that the sensor will retrieve only the reflectance values reflected from particles and not their total concentration or the water's reflectance values. They concluded that indeed the algorithm had a great performance with minor problems occurring when different particle sizes concentrations were involved and specific calibration was needed to avoid fluctuation of errors.

Another characteristic that must be taken into consideration when applying turbidity algorithms is the overall behaviour of dams and lakes in terms of reflectance during seasonal changes. Hadjimitsis, Hadjimitsis, Clayton and Clarke (2006, p. 459) stated that Kourris dam, Cyprus, had strong correlation of turbidity with remote sensed data of Landsat 5 TM's band 3. They observed that during winter season, reflectance for Landsat 5 TM's band 3 retrieved an increment up to 5% compared to autumn and spring seasons where reflectance fluctuated to lower values 4% and 3%, respectively. As algorithms are applied after atmospheric correction, the utilisation of the correct reflectance values that match to the dam's spectral profile is crucial and an important factor to determine turbidity concentrations.

3 Methodology

3.1 Introduction

This chapter explains the principles and methods used for the pre-processing of raw satellite images up to the final stage of post-processing. In total, 15 digital images of the two dams were acquired for years of 2006 to 2016 and then they were processed in order to retrieve Chl-a and turbidity concentrations as well as TSI values. For every year, up to three digitals images were selected to investigate the abovementioned parameters considering mostly the summer and winter seasons of each year.

Furthermore, ENVI software was used to convert digital images' Digital Numbers to Radiance. Thereafter, Fast Line-of-sight Atmospheric Analysis of Spectral Hypercubes (FLAASH) was applied to perform atmospheric correction and retrieve reflectance values.

3.2 Study areas & Climate Characteristics

Both dams, Asprokremmos and Kouris, are the largest from totally 108 dams varying from small ponds to major dams in Cyprus, with the latter to be the largest. Asprokremmos dam is located East near Paphos city, it has an overall capacity of 52,375,000 cubic meters and it is supplied by the river Xeros (Papoutsa et al, 2012, pp.25-26). Kourris dam is positioned North East near Limassol city with a total capacity of 115,000,000 cubic meters (Bororinam, Renard, Balderer & Christodoulides, 2003, p. 130) and it is supplied by three rivers, Kryos, Limnatis and Kouris with the latter being the largest river in Cyprus.

The country'climatology is categorised as an intense Mediterranean climate with regular and repeated droughts. Along that, evapotranspiration of fresh water is also observed to be in high rates, up to 86%, due to long summers and short winters with low rainfall (Water Development Department, 2002, p.3).

Figure 3.1: Indicates the south-eastern part of the island Cyprus and its two largest dams, Asprokremmos (left) and Kourris (right).

3.3 Pre-processing and Post-processing of Satellite Images

Satellite images derive from the satellite's calibrated sensors as raw images. Due to the fact that satellites are located in a constant orbit, altitude and speed around the earth, several important errors produced from the aforementioned factors must be calibrated in order to retrieve accurate results at a further stage. The processing starts with the retrieval of the digital image from electronic archives owned by scientific institutions such as National Aeronautics and Space Administration (NASA) and European Space Agency (ESA). The next steps of pre-processing are explained at the following subchapters.

3.3.1 Geometric Calibration

Mainly, due to the movement and vibration caused during the launch of Space Rockets, it is common that sensors on satellites and afterwards the digital images to present geometric errors. Some of the errors are also produced due to mechanical equipment's imperfections such as incorrect establishment and calibration of the lens or, rarely, deviation due to manufacturing processes. Other errors can be also produced due to incorrect mathematical calculations regarding the satellites movements when they orbiting earth. In addition, the utilisation of specialised software can be used when it is known that there is a systematic

image error. Systematic image errors are mostly produced from sensor or camera movements and the reference ground points used for calibration of the device. Fortunately, most of the satellites are mechanically capable to correct the most of the aforementioned errors utilising different methods from ground control points (Jacobsen, n.d., p.1).

3.3.2 Digital Numbers & Radiance

According to Centre of Remote Imaging, Sensing and Processing (2001, para 5), digital images are consisted in terms of pixels. Pixels are actually the geographical representation of the earth mapped at the image and its resolution depends on the sensor's manufacturing properties, for example 30m x 30m resolution. Each pixel is measured in digital number which characterises the intensity value of the solar radiance reflected, emitted or backscattered from the ground. In addition, the intensity of the pixel is generally measured as 0 to represent the black and 255 the white colour.

These numbers at the stage of processing are not yet meaningful and measurable units. Therefore, the conversion of digital numbers to radiance values must be done in order to retrieve the average reflectance of each pixel while the next step of image processing is called radiometric calibration (Harris Geospatial Solutions, 2013, para 4).

For each satellite's sensors, different calibrated formulas are used. According to Finn, Reed and Yamamoto (n.d., pp.2-3), the conversion of digital numbers to radiance values are applied to each band to ensure that the outcome will be equally distributed no matter of the study's purpose. The following equations represent the formula used for each satellite that was used in this study.

For Landsat 5 TM: $$L_\lambda = G_{rescale} \times DN + B_{rescale} \quad (3.1)$$

Where L_λ is the radiance, $G_{rescale}$ is the band specific rescaling gain factor, DN is the Digital Number and $B_{rescale}$ is the Band specific rescaling bias factor. All this information except of digital numbers can be found in the metadata archives and the values of gain and bias factors were usually constants according to the satellite's sensors updating, dating back to 1984, 2003 and 2007.

For Landsat 8: $L_\lambda = M_L \times Q_{cal} + A_L$ (3.2)

Where L_λ is the Spectral radiance, M_L is the Radiance multiplicative scaling factor of the band, A_L is the Radiance additive scaling factor of the band, both found in the metadata archives of the satellite image. Q_{cal} is the pixel value in digital number (USGS, 2016).

The utilisation of specialised software such as ENVI, computes the abovementioned equations depending on the satellite's acquisition image and the outcomes are images converted to radiance. The 15 acquired digital images were converted from digital numbers to radiance as the first step of pre-processing. The following table describes the characteristics of the digital images obtain by USGS.

Table 3.1: Shows the main characteristics of each digital images.

No	Satellite	Acquisition Date	Resolution & Bands Used
1	Landsat 5 TM	16/SEP/2006	RGB for Landsat 5 TM 30m x 30m Aerosol & RGB for Landsat 8 OLI
2	Landsat 5 TM	4/SEP/2007	
3	Landsat 5 TM	23/JUL/2009	
4	Landsat 5 TM	25/SEP/2009	
5	Landsat 5 TM	28/NOV/2009	
6	Landsat 5 TM	5/APR/2010	
7	Landsat 5 TM	27/AUG/2010	
8	Landsat 5 TM	14/OCT/2010	
9	Landsat 5 TM	8/APR/2011	
10	Landsat 5 TM	13/JUL/2011	
11	Landsat 8 OLI	24/MAR/2013	
12	Landsat 8 OLI	22/AUG/2014	
14	Landsat 8 OLI	24/JUL/2015	
15	Landsat 8 OLI	13/NOV/2015	
16	Landsat 8 OLI	8/JUN/2016	

3.3.3 Top of the Atmosphere and Reflectance – FLAASH

Top of the Atmosphere (TOA) correction actually means the removal of effects caused outside the earth's atmosphere. Such examples are errors caused by the curvature and refraction due to earth's atmosphere. Besides that, ENVI software includes and performs TOA correction during the conversion of radiance values to reflectance values.

To retrieve reflectance, the next step of pre-processing leads to atmospheric correction where the atmosphere's effects such as aerosols and particles are removed from the digital image. More specifically, Mousivad, Verhoef, Menenti and Gorte (2015, p.8021) stated that

reflectance can be also affected by topographic characteristics of the terrain being studied. The optical depth where the altitude between ground elevation and sensor's position determines the increment or decrement of aerosols and gases, the terrain morphology where it determines the type of scattering of irradiance and the fraction caused by the atmosphere and the sun.

Mainly, reflectance depends on three major factors. The first is the illumination of irradiance caused by the earth's surface, the second is the reflectance produced by the earth's surface and the third is the path of radiance. The following equation summarises how reflectance can be obtain mathematically.

Reflectance: $$(L_{sat}) = [\tau_v (\tau_o E_o \cos\theta_o + E_{sky})] R_{RS}(\theta_v) + L_* \quad (3.3)$$

Where E_o is the solar constant, τ_o is the atmospheric transition along the sun-ground path, τ_v is the atmospheric transition along the ground-detector path, θ_o is the solar zenith angle, E_{sky} is the irradiance at the earth's surface due to skylight, $Ed = \tau_o E_o \cos\theta_o + E_{sky}$ is the total irradiance at the earth's surface, θv is the observation angle and L* is the path angle (Philpot, 2014).

FLAASH is an advanced tool included in ENVI software package. FLAASH during analysis of digital images utilises the MODerate resolution TRANsmission code (MODTRAN) which is capable to calculate the line of sight of atmospheric spectral transmittances and radiance uniquely for every digital image. A variety of parameters including climatology of the terrain acquired with the image from the satellite as well as the calculation of parameters such as molecular and particulate absorption, emission and scattering, the surface reflection and emission, the solar illumination and finally spherical refraction is performed during the analysis (Spectral Sciences Incorporated,2016, para 2).

Validation of the 15 digital images' reflectance values were done with the comparison between NASA's image processing algorithms with the results derived from this study. It was decided to follow this way of validation as many input parameters were unavailable and needed time consuming efforts to ensure that the parameters were correct for every digital image. Truth data was also unable to be collected as specialised equipment such as a boat to access both dams were unavailable.

3.3.3 Selection of Algorithms

The algorithms used for this study were mainly chosen according to the satellites' sensors characteristics, for example digital images originated from Landsat 5 TM led to the utilisation of calibrated algorithms which had the same bands characteristics. In certain cases, where calibrated algorithms for the particular dams were not found, such as Chl-a algorithms, the selection was made by empirical assumptions and common characteristics concerning other dams and lakes.

Besides that, Asprokremmos and Kourris dams share similar spectral profiles as well as validated truth data collected by studies where algorithms were established. Thus, the final results were described as approximate values rather than correlated and accurate values. The following table describes the bands characteristics of each satellite that was utilised for the purpose of this study.

Table 3.2: **Summarises the satellites' bands wavelength characteristics.**

	Landsat 5 TM (μm)		**Landsat 8 OLI (μm)**
Band 1(Blue)	0.45-0.52	Band 1(Aerosol)	0.43-0.45
Band 2(Green)	0.52-0.60	Band 2(Blue)	0.45-0.51
Band 3(Red)	0.63-0.69	Band 3(Green)	0.53-0.59
Band 4(NIR)	0.77-0.90	Band 4(Red)	0.64-0.67
-	-	Band 5(NIR)	0.85-0.88

Source: USGS, n.d..

For turbidity, $y = 2.897x - 0.247$, x = band 3 (NTU) (3.4)

The algorithm was mainly developed and calibrated for Landsat 5 TM and CHRIS/PROBA by Papoutsa et al (2014, p.1688) concerning the Asprokremmos dam. Several in-situ samples were collected during selected dates that Landsat 5 TM and CHRIS/PROBA overpassed the area. In this study, the same algorithm was also utilised for Landsat 8 OLI digital images in order to observe its overall efficiency for both dams.

For TSI, $TSI = 100*\exp(-0.24*(\text{band 2}/\text{band 3}))$ (3.5)

The algorithm was developed utilising the spectroradiometer GER 1500 by acquiring 18 in-situ samples from Asprokremmos dam, 5 samples for both Alyki (Larnaka) and the open sea in Cyprus and finally 10 samples from Lake Karla, Thessaly in Greece. It can be used for satellites which their spectral bands were designed for 350 nm to 1050nm and it is more

correlated with turbidity, especially with Secchi Disk (Papoutsa, Akylas, Hadjimitsis, 2014, pp. 71-72).

Algorithm (3.6) below was calibrated and created for Landsat 7 ETM+ concerning as study area the West Lake in China (Torbick et al, 2008). For this study, it was utilised for Landsat 5 TM as the two satellites share the same band characteristics. Algorithm (3.7) was exclusively calibrated and utilised for Landsat 8 OLI satellite and Jordan Lake, United States (Yand & Anderson, 2016).

For Chl-a, $Chl\text{-}a = (5.009*(Band3/Band1))-1.855$ (3.6)

$Chl\text{-}a = (7.7555*(alog(Band3/Band1)))+1.1738$ (3.7)

4 Results & Discussion

4.1 Introduction

The following chapter presents the final results retrieved from the four proposed algorithms. More specifically, validation of reflectance values was done by the utilisation of in-situ data acquired from other studies. The estimated data retrieved from the post-processed images such as the classification of the trophic states, turbidity and chl-a values, were justified mainly by the monthly rainfall records produced by the Department of Meteorology and other studies. Possible source of errors are also mentioned in this chapter appointing their significance and impact at the final results.

4.2 Main Assumptions

Firstly, due to the fact that no in-situ data were possible to be obtained for all the acquired images, the final parameters' values were assumed to be estimated data. Consequently, they were expected to fluctuate similarly with values presented by other studies concerning the two dams. In case of no similar matching such as higher concentrations between the actual in-situ data and this study's estimated data, an approximate approach of justification was made by utilising rainfall records up to a period of past three months. It was assumed that the overall rainfall collected at higher altitude which afterwards supplied the dams' rivers, was the main supply of nutrients and suspended particles in the dams, for Chl-a and turbidity respectively.

4.3 Validation of Reflectance Values

Mainly four in-situ spectral signatures were obtained in order to be compared with this study's reflectance values from the ENVI software. The spectral signatures were acquired at Asprokremmos dam on the 27th of August and 14th of October in 2010 by Dr. Papoutsa (2015) with exact coordinates 34°45'15.3"N - 32°34'28.1"E (Inlet) and 34°43'38.4"N - 32°33'13.6"E (Outlet), latitude and longitude for both respectively.

According to the table below, it can be observed that at the exact coordinates of outlet sampling station, reflectance values were closely matched between in-situ and estimated data with minor variations. It can be said that atmospheric correction for these digital images performed well. For the remaining digital images, the variation of reflectance values was

expected to fluctuate 3-6% for band 1, for 6-12% for band 2 and 4-7% for band 3 considering increment and decrement due to seasonal changes.

Table 4.1: Indicates the in-situ compared with the estimated reflectance values.

	Mean Reflectance Values					
Date	**Papoutsa (2015)**					
	Inlet (34°45'15.3"N-32°34'28.1"E)			**Outlet (34°43'38.4"-32°33'13.6"E)**		
27/AUG	Blue 0.485 μm	Green 0.569 μm	Red 0.660 μm	Blue 0.485 μm	Green 0.569 μm	Red 0.660 μm
	3.89%	6.27%	5.99%	1.97%	3.88%	1.17%
	ENVI					
	Inlet (34°45'15.6 N – 32°34'20 E)			**Outlet (34°43'38.5 N–32°33'14 E)**		
	Blue 0.485 μm	Green 0.569 μm	Red 0.660 μm	Blue 0.485 μm	Green 0.569 μm	Red 0.660 μm
	4.12%	7.39%	5.58%	2.95%	4.52%	3.09%

	Mean Reflectance Values					
Date	**Papoutsa (2015)**					
	Inlet (34°45'15.3"N-32°34'28.1"E)			**Outlet (34°43'38.4"-32°33'13.6"E)**		
14/OCT	Blue 0.485 μm	Green 0.569 μm	Red 0.660 μm	Blue 0.485 μm	Green 0.569 μm	Red 0.660 μm
	4.97%	7.67%	5.03%	3.39%	5.08%	2.13%
	ENVI					
	Inlet (34°45'15.6 N – 32°34'20 E)			**Outlet (34°43'38.5 N–32°33'14 E)**		
	Blue 0.485 μm	Green 0.569 μm	Red 0.660 μm	Blue 0.485 μm	Green 0.569 μm	Red 0.660 μm
	8.74%	10.17%	6.32%	3.28%	4.11%	2.06%

Source: Papoutsa, (2015); Papoutsa & Hadjimitsis (2014).

In addition, it was also expected that reflectance values would present errors derived by the provision of incorrect input parameters such as visibility to the software. Other source of errors were also assumed to be presented due to the evaporation of the water mass in the dam and satellites sensor's limitations such as spectral and spatial resolution.

To ensure that all pre-processed images were atmospherically corrected properly and that reflectance values were reasonable, several images corrected by NASA's algorithms were obtained and compared for validation purposes. It was observed that the acquired digital images of this study shared the same reflectance values with minor variations of bands' reflectance values. For example, there were difference up to 1-1,5% between the compared images and they were accepted as correct.

4.3 Results & Discussion– Chl-a and Turbidity

Turbidity, Chl-a and TSI algorithms were applied after the pre-processing of the 15 digital images and it was expected that Turbidity parameter would present a strong correlation with TSI. On the other hand, minor concerns arise for Chl-a eutrophication detection by the TSI algorithm as its development was based more on the turbidity parameter. Another concern was that there is not an algorithm for Chl-a to be established for the both dams, therefore the chosen algorithms from literature were expected to present, in some cases, non-logical Chl-a concentration values.

More specifically, in order to estimate and quantify accurately the behaviour of both dams, mean values of all parameters were collected through the 15 pre-processed images by utilising the region of interest tool of ENVI 4.8 software package. The main idea was to collect average values from a number of pixels at three locations of the dams, inlet, middle and outlet. At each location, it was expected that parameters' concentrations would fluctuate as the empirical in-situ data collected by Papoutsa & Hadjimitsis (2014), Papoutsa, Akylas & Hadjimitsis (2014), Papoutsa (2015).

It should be mentioned that in specific months, the water level of both dams altered due to droughts and overflows and therefore the region of interest was never at the same location, especially the inlet location.

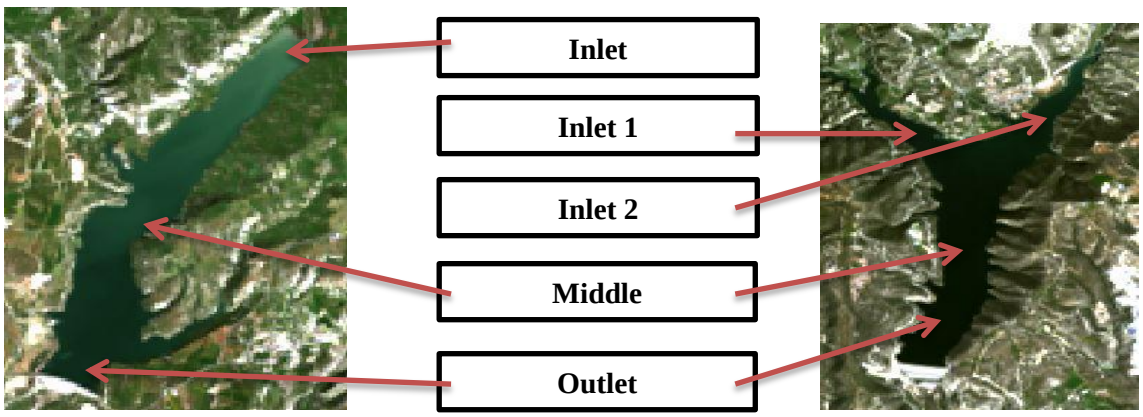

Figure 4.1: Presents the inlet, middle and outlet locations for both dams, where mean values for all parameters were obtained.

The expectation was that turbidity would fluctuate up to 5-15 NTU for Asprokremmos dam. Regarding the inlet locations, it was expected that higher values would be presented mostly due to rivers estuaries supplying turbid water and shallow in depth water areas. With the same principle, Chl-concentrations were presumed to vary up to an average 20 mg/L.

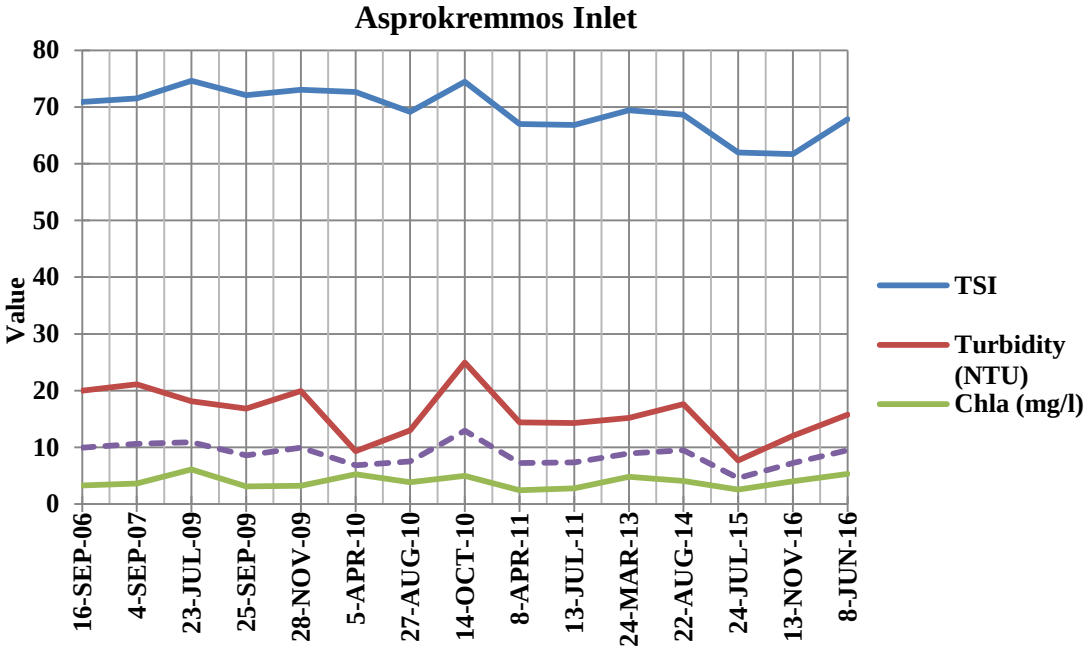

Figure 4.2: Illustrates TSI, turbidity and Chl-a concentrations at inlet locations of Asprokremmos Dam for each date.

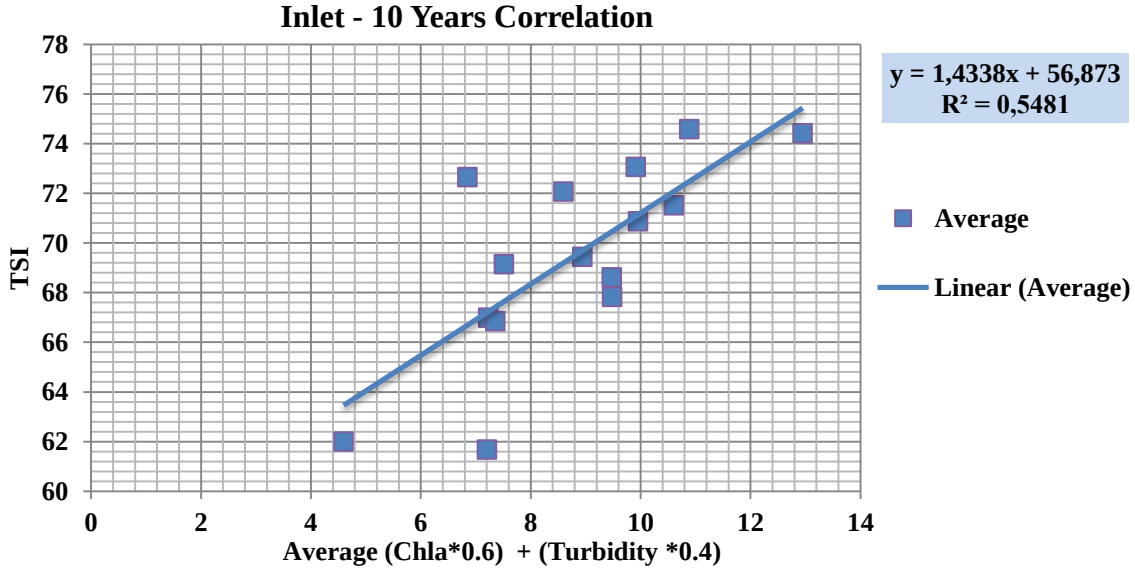

Figure 4.3: Illustrates the ten year correlation of TSI with the average model's best fit line at inlet locations of Asprokremmos Dam.

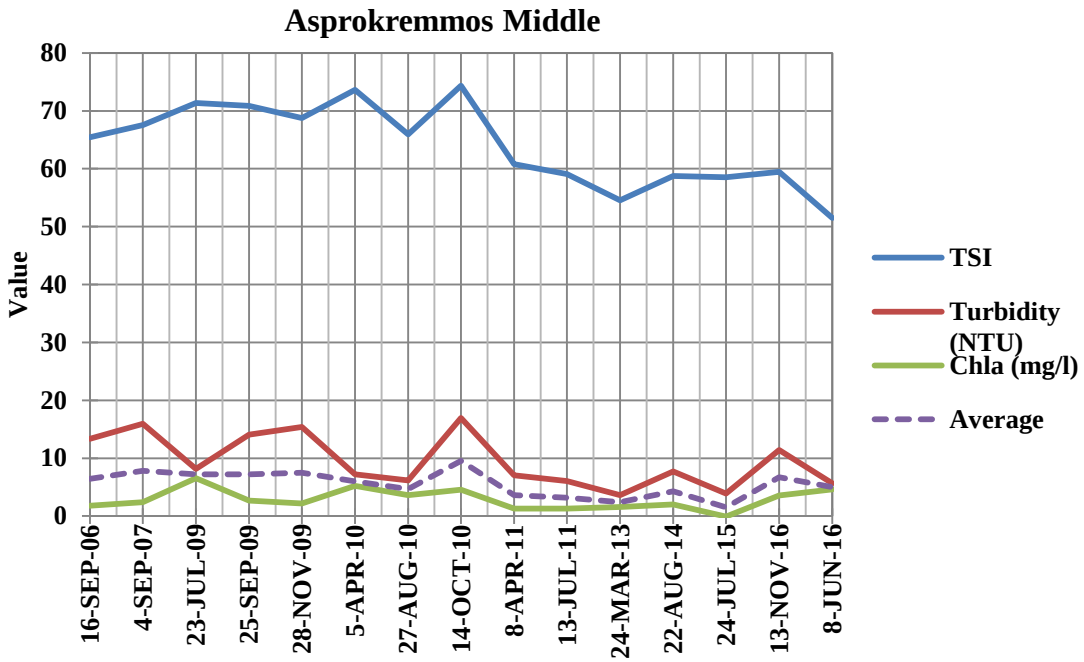

Figure 4.4: Indicates TSI, turbidity and Chl-a concentrations at middle locations of Asprokremmos Dam for each date.

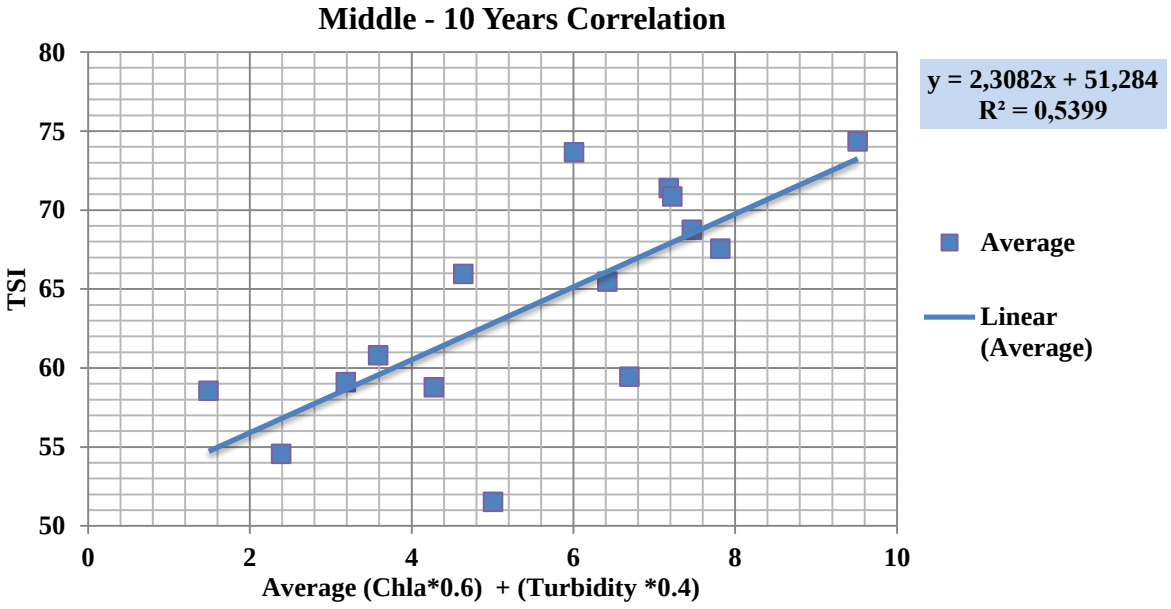

Figure 4.5: Indicates the ten year correlation of TSI with the average model's best fit line at middle locations of Asprokremmos Dam.

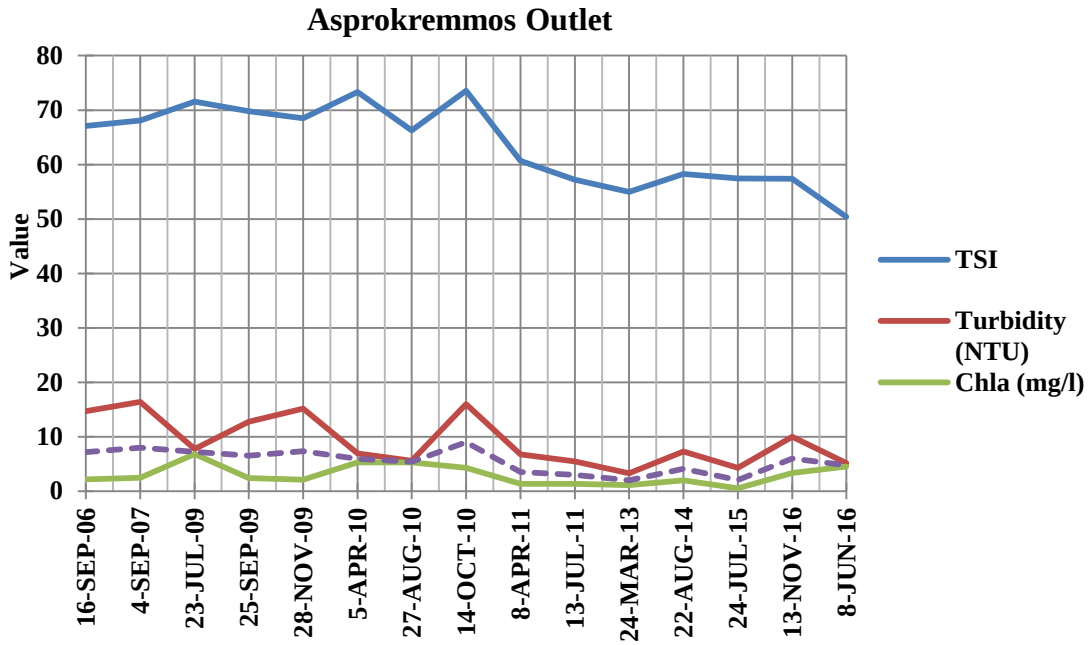

Figure 4. 6: Shows TSI, turbidity and Chl-a concentrations at outlet locations of Asprokremmos Dam for each

date.

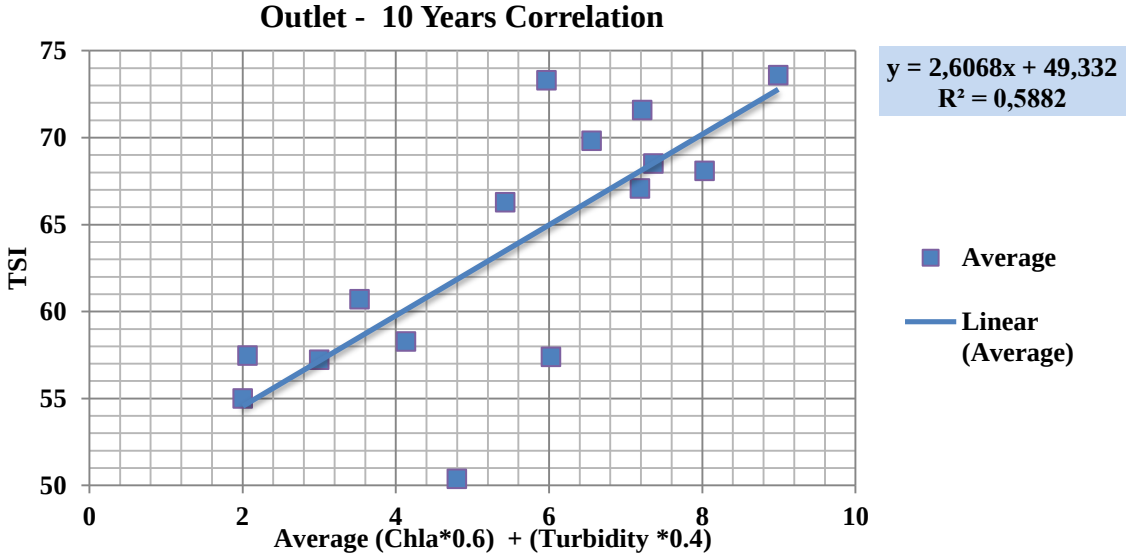

Figure 4.7: Shows the ten year correlation of TSI with the average model's best fit line at outlet locations of Asprokremmos Dam.

As it can be inferred from figures 4.2, 4.4 and 4.6, it is clearly obvious that turbidity and Chl-a for Asprokremmos dam correlated with TSI values. More specifically, where TSI values indicated peaks is where turbidity and Chl-a presented an independent increment in concentrations and vice versa. This can lead to the conclusion that the proposed TSI algorithm performs as well as for the detection Chl-a concentrations. Moreover, the dashed line signifies the best fit line at each location based on a linear regression model weighting 0.60 for Chl-a and 0.40 for turbidity values (e.g. [Chl-a x 0.60] + [turbidity x 0.40]).

Furthermore, the correlation of TSI values regarding the linear regression models was found to score up to 0.59 leading to a preliminary conclusion that the gap of time between the examined dates influenced the overall distribution of the parameters mean values. In addition, for a ten year period, the overall amount of processed images is inadequate to achieve higher correlation.

In terms of parameter's concentrations at Asprokremmos dam, it was observed that turbidity values indicated high concentrations in general, up to 20-25 NTU during winter to spring seasons (e.g. end of 2009 to mid-spring 2010), particularly at middle and outlet locations. This can be explained by the fact that river Xeros pass through a geological soft soils area such as sands, silts, clays and gravels (Geological Survey Department, 2016).

During rainy seasons and snow melting, large quantities of water drags nutrients and suspended particles with final destination to be at the dam. On the other hand, Chl-a concentrations seemed to be increased as turbidity indicated decrement during seasons that water entered the dam with minor or no quantities (e.g. autumn 2007 to mid-summer of 2009). Moreover, the combination of continuous solar irradiance and high temperatures for long periods of time, Chl-a increased its concentrations.

Table 4.2: Presents average rainfall at Paphos (Airport) and Pano Panagia of Troodos mountain, an area where river Xeros has its main supply of water.

Month/Year	Monthly Rainfall	
	Pano Panagia	Paphos (Airport)
December/2009	146% (Overall in Cyprus)	
January/2010	123%	113%
February/2010	117%	70%
November/2012	145%	201%
December/2012	242%	173%
January/2013	56%	56%

Source: Department of Meteorology, 2016.

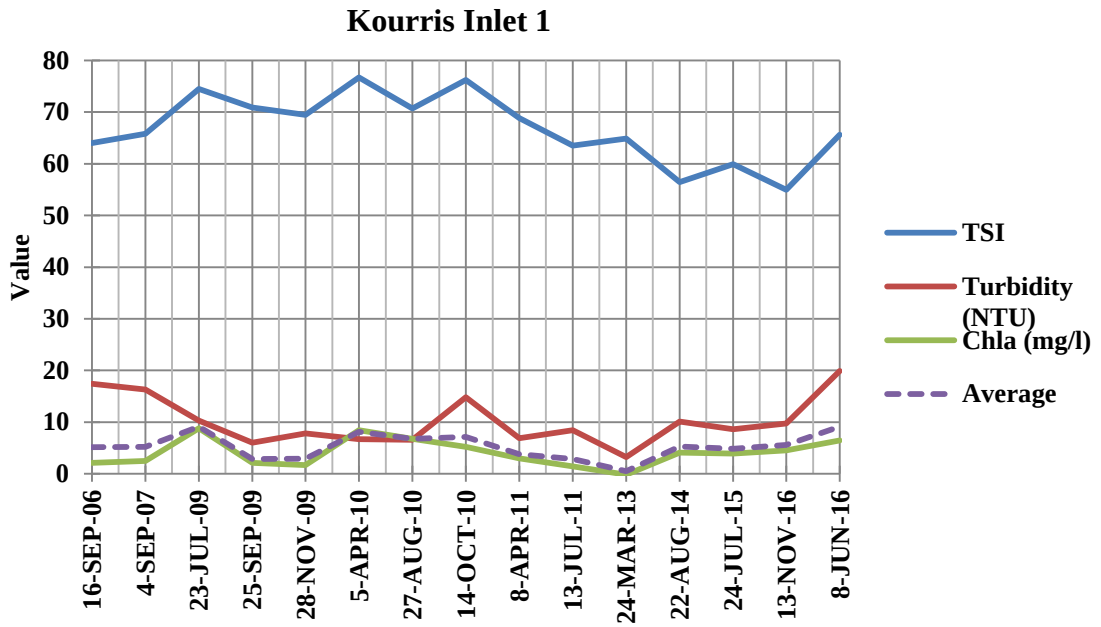

Figure 4.8: Illustrates TSI, turbidity and Chl-a concentrations at inlet 1 locations of Kouris Dam for each date.

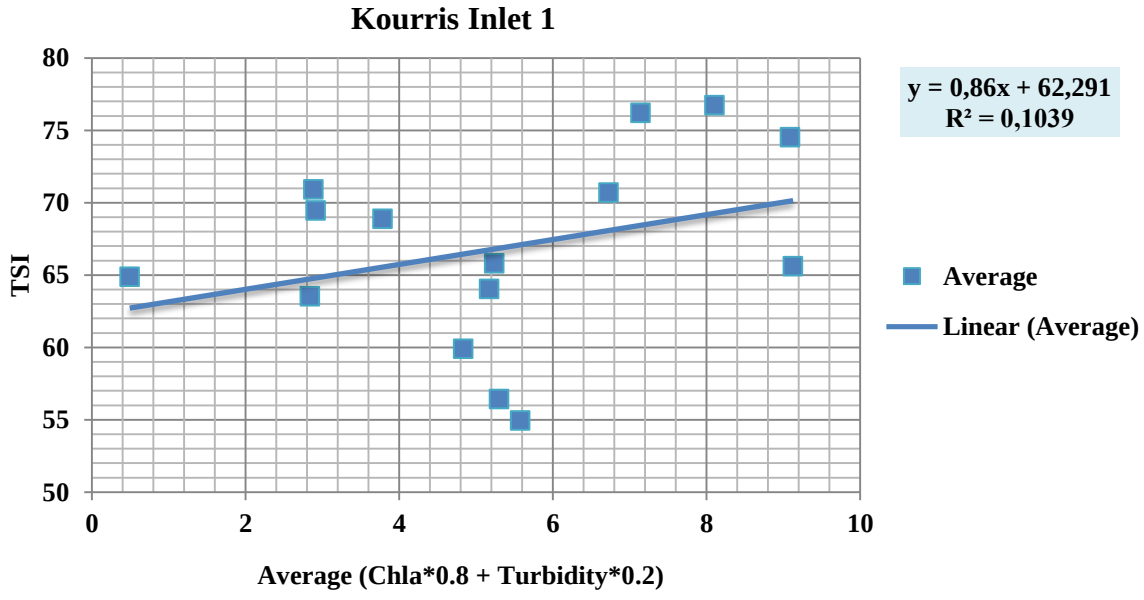

Figure 4.9: Illustrates the ten year correlation of TSI with the average model's best fit line at inlet 1 locations of Kourris Dam.

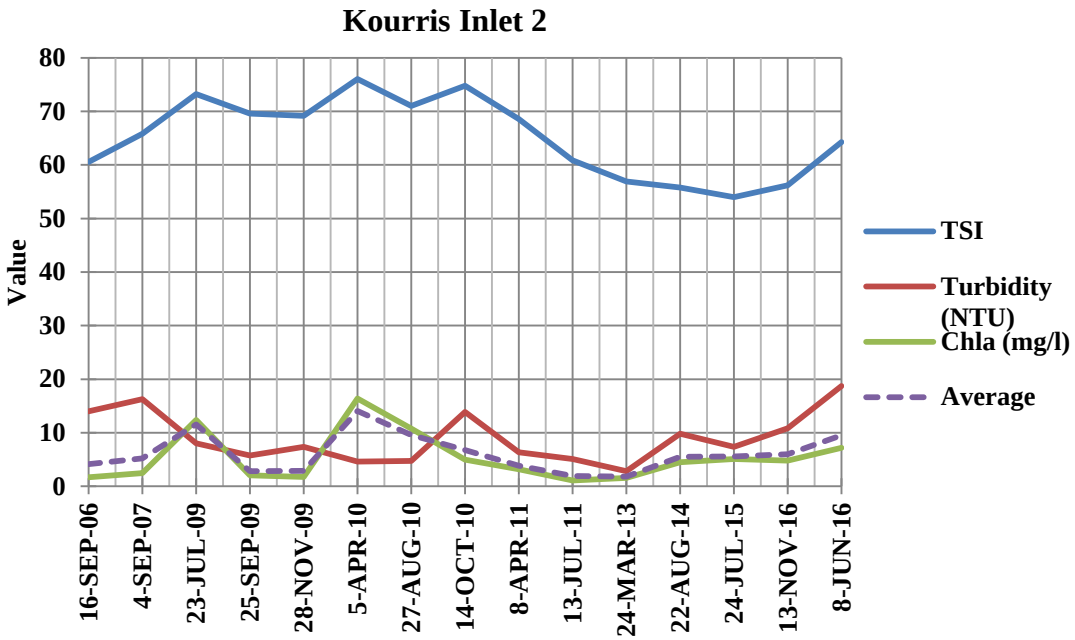

Figure 4.10: Indicates TSI, turbidity and Chl-a concentrations at inlet 2 locations of Kourris Dam for each date.

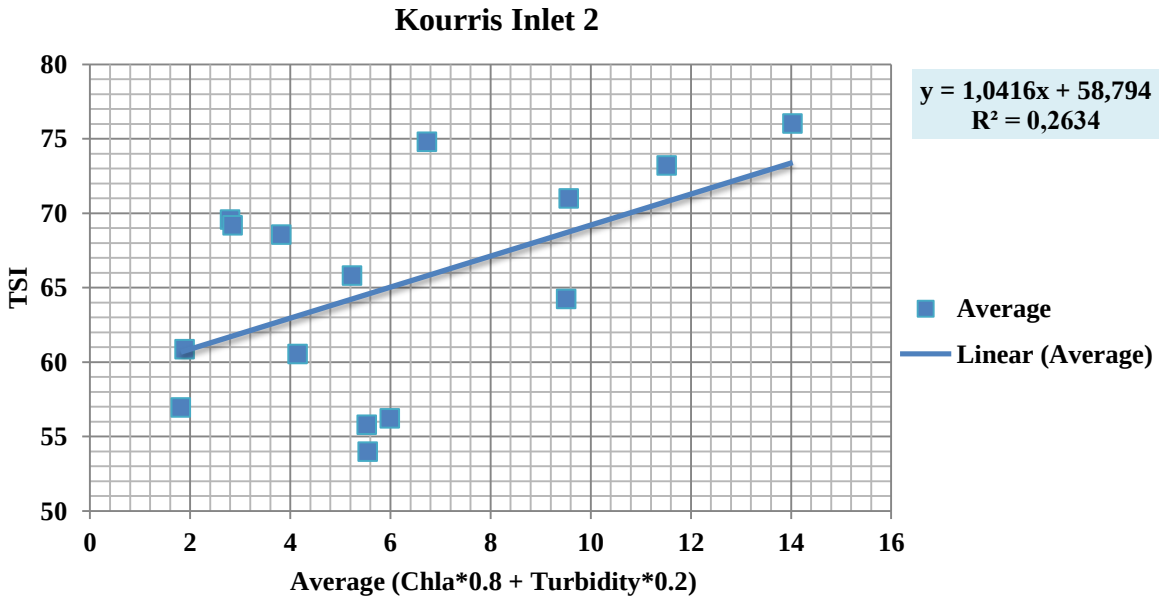

Figure 4.11: Indicates the ten year correlation of TSI with the average model's best fit line at inlet 2 locations of Kourris Dam.

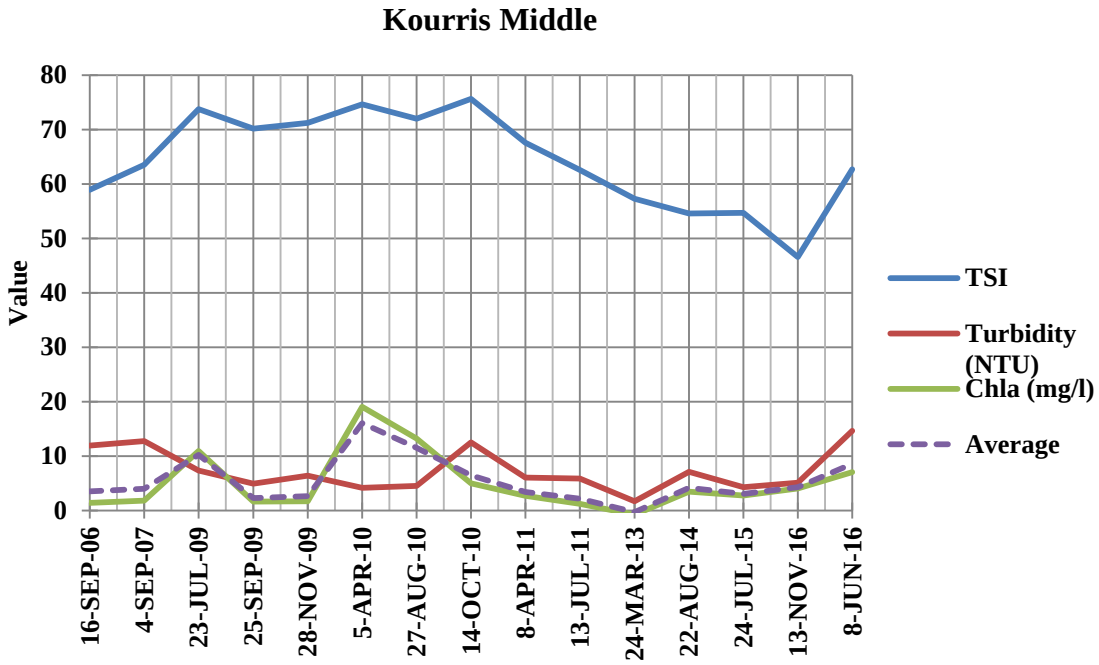

Figure 4.12: Shows TSI, turbidity and Chl-a concentrations at middle locations of Kourris Dam for each date.

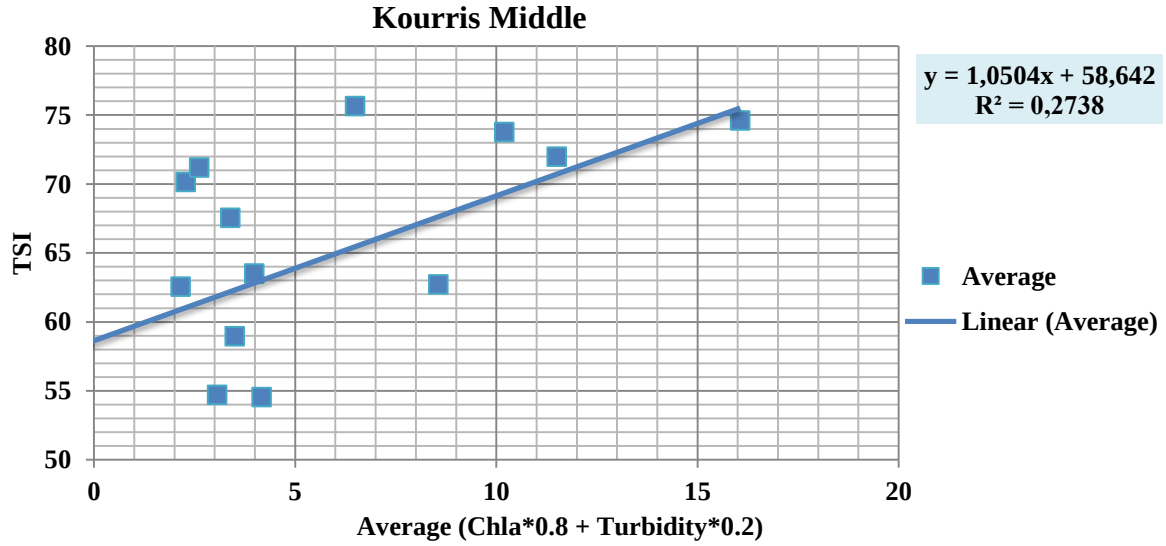

Figure 4.13: Shows the ten year correlation of TSI with the average model's best fit line at middle locations of Kourris Dam.

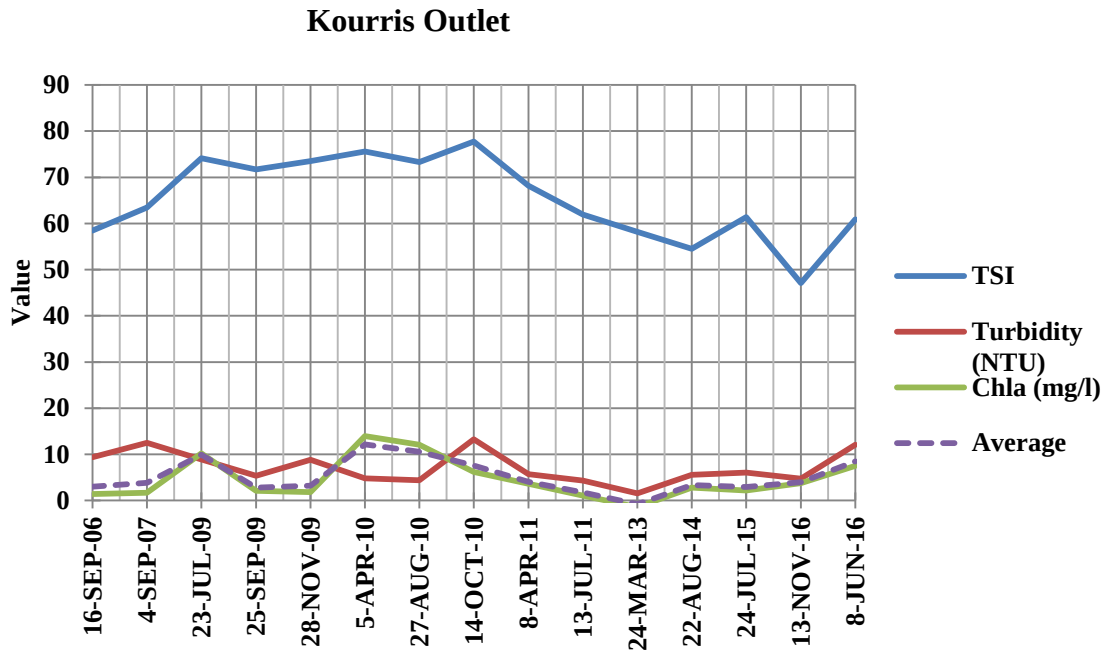

Figure 4.14: Presents TSI, turbidity and Chl-a concentrations at outlet locations of Kourris Dam for each date.

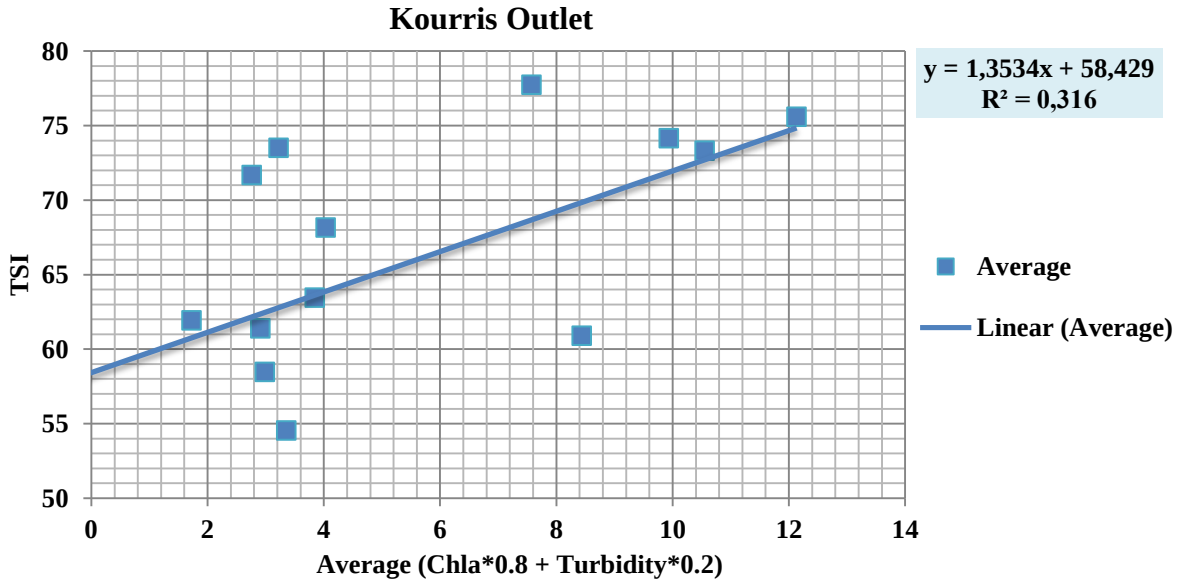

Figure 4.15: Presents the ten year correlation of TSI with the average model's best fit line at outlet locations of Kourris Dam.

Observing the figures 4.8 to 4.15, it can be stated that Turbidity concentration values at Kourris dam generally indicated lower results than that obtained from Asprokremmos dam. More precisely, the higher mean value, 16 NTU, was found at both inlet locations of Kourris dam whereas Asprokremmos dam showed up to 23 NTU at the same location. A factor that may influence turbidity concentrations at Kourris dam resulting to be lower is the fact that the rivers pass through a stiffer geological area than this of Asprokremmos dam. It is important to be mentioned that the final results are quite rational and that the turbidity algorithm priamrly used for Asprokremmos dam also performs well for Kourris dam.

Furthermore, it can be observed that both dams share a similar pattern of all parameters' concentration increment and decrement during seasonal changes with Asprokremmos dam to be more sensitive with sharper peaks. As stated in subchapter 'study areas and Climate Characteristics', the aforementioned dam is the second larger and has the half capacity of Kourris dam. Therefore, its morphology favours and easier increment and vice versa of parameters concentrations.

The algorithms utilised for the detection of Chl-a concentrations and the assumption that Kourris dam overall average values would fluctuate up to 20 mg/L, led to the conclusion that the algorithms performed well for both dams. In addition, the linear regression models ([Chl-a*0.8] + [Turbidity*0.2]) showed a correlation up to 0.37 with TSI values. In the case of Kourris dam, it was observed that after atmospheric correction, the reflectance values for Band 1 fluctuated at non-normal values, near 0%. Consequently, when the two-band Chl-a algorithms were applied, the outcome led to near zero or excessively higher than the normal concentrations values e.g. mostly seen at 5th of April, 2010 and 23rd of March, 2013. An important factor which caused the final output, it was the application of the same weather parameters (e.g. visibility) for both dams since the two investigated area were processed as one single digital image.

Table 4.3: Presents average rainfall at Saittas Village and Limassol.

Month/Year	Monthly Rainfall	
	Saittas Village	Limassol
December/2009	146% (Overall in Cyprus)	
January/2010	119%	131%
February/2010	123%	96%
November/2012	185%	126%
December/2012	226%	178%
January/2013	61%	36%

Source: Department of Meteorology, 2016.

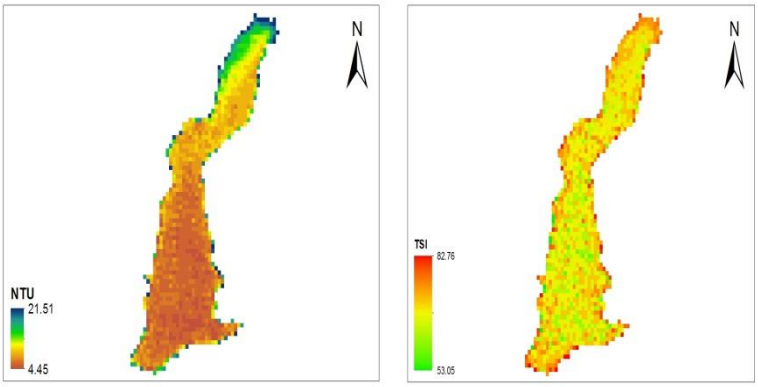

Figure 4.16: Indicates the final maps concerning turbidity and TSI for Asprokremmos dam at 23rd of July, 2009.

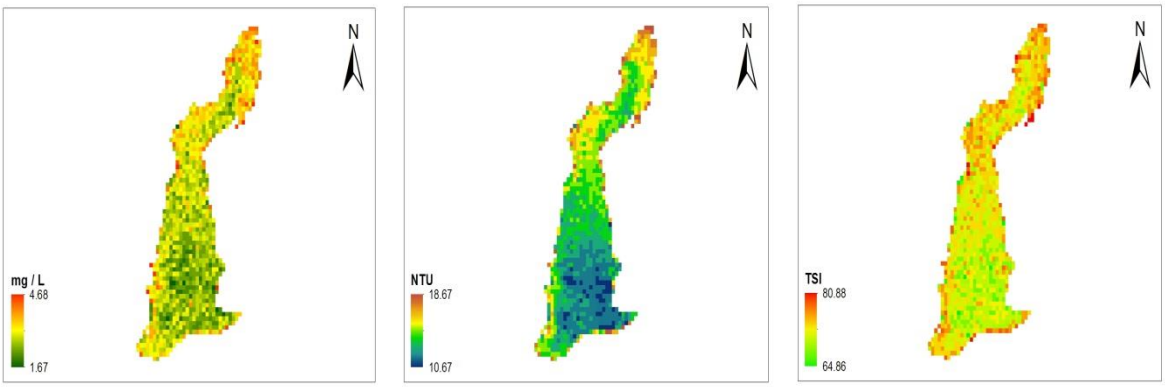

Figure 4.17: Indicates the final maps concerning Chl-a, turbidity and TSI for Asprokremmos dam at 25th of September, 2009.

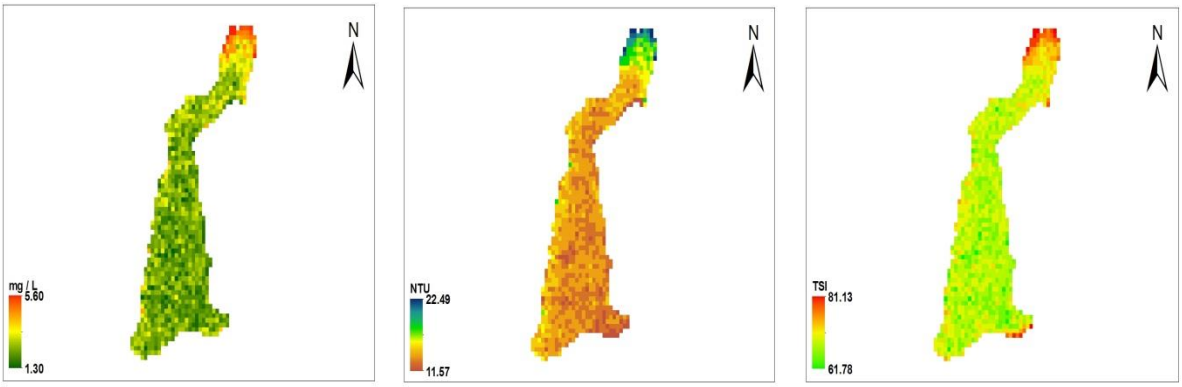

Figure 4.18: Indicates the final maps concerning Chl-a, turbidity and TSI for Asprokremmos dam at 28th of November, 2009.

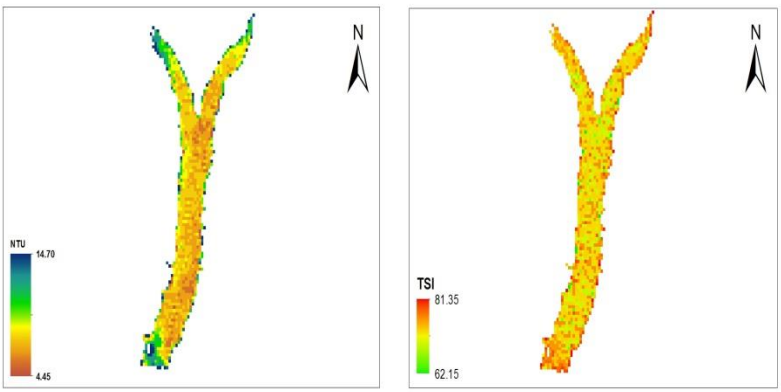

Figure 4.19: Illustrates the final maps concerning turbidity and TSI for Kourris dam at 23rd of July, 2009.

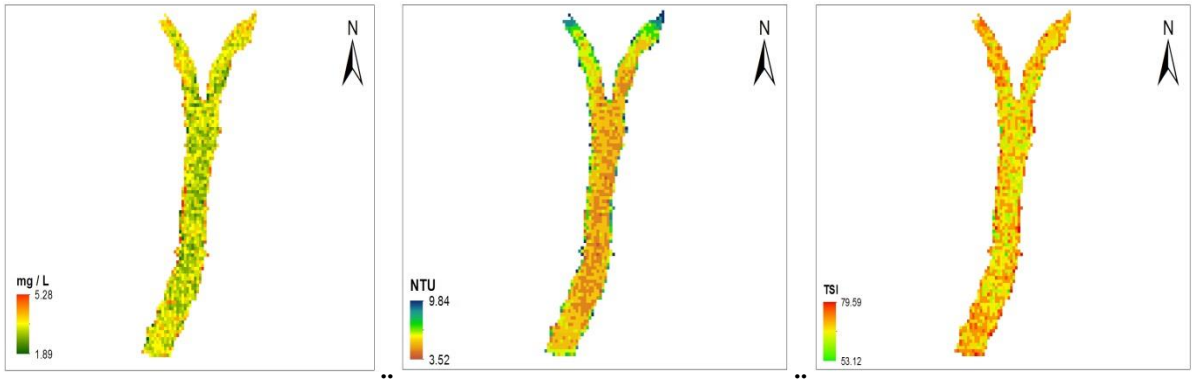

Figure 4.20: Presents the final maps concerning Chl-a, turbidity and TSI for Kourris dam, at 25th of September, 2009.

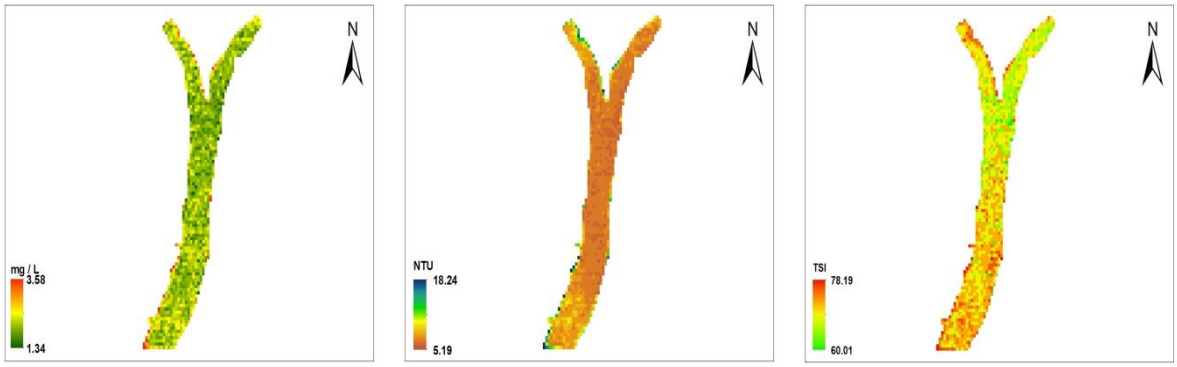

Figure 4. 21: Presents the final maps concerning Chl-a, turbidity and TSI for Kourris dam at 28th of Novemeber, 2009.

The figures above indicate the overall surface concentrations for all parameters regarding both dams. As it can be observed, both dams share the same characteristics. High turbid waters and high Chl-a concentrations were found at inlet locations, as it was firstly assumed, whereas lower concentrations found to be at the middle and outlet of both dams. In addition, as TSI is a combination of Chl-a and turbidity as independent parameters, it can be concluded that it clearly indicate the parameters' eutrophication.

In addition, the two different dates illustrates the seasonal difference between them. Such an example is the increment of turbidity concentrations, from 4.45 NTU at 23rd of July to 10.67 NTU at 25th of September, as water entered the Asprokremmos dam at the latter date. For TSI, this seasonal change resulted to a decrement of eutrophication, mostly seen at the overall surface of the dams. More specifically, the majority of pixels classify the dams as eutrophic ranging from 50 to 70. Finally, it can be concluded that as mentioned in previous statement that indeed Chl-a influences TSI sensitivity more than turbidity.

5 Conclusion

5.1 Main concluding remarks

In this study, water quality parameters and their characteristics were examined regarding the two biggest dams in Cyprus, Asprokremmos and Kourris. An extensive literature was carried out mentioning the most important parameters considered when Chl-a and turbidity concentrations develop and impact environmentally the overall quality of an inland water body.

Ten digital images from Landsat 5 TM and five from Landsat 8 OLI were acquired for processing purposes of the aforementioned dams covering a ten year period. As a part of pre-processing the satellite images, radiometric and atmospheric corrections were performed to retrieve reflectance values. Chl-a, turbidity and TSI values were obtained by the utilisation of four proposed algorithms.

Observing the final estimated results, it was concluded that the ten year approach for both dams showed good estimation of turbidity concentrations reaching up to 5 to 20 NTU for three selected region of interests. Justification was done by the collection of data from other studies' campaigns empirical data mostly for Asprokremmos and as it was not possible to acquire detail in-situ concentration values starting from 2006 and ending in 2016. In addition, the presentation of tables describing weather meteorological data up to 3 months before the acquired dates, were also presented in order to justify increment and decrement of parameters' concentrations.

Following the same principles, Chl-a concentrations were observed to fluctuate at reasonable estimated average values, up to 20 mg/L, as it was assumed for Asprokremmos and Kourris dams. For Kourris dam, the utilisation of the same weather parameters during atmospheric correction at both dams influenced Band 1 (Blue) which is the nearest band to aerosols' removal. This resulted with relatively lower reflectance values than the normal and subsequently, a number of specific processed images presented lower or higher concentrations. Considering the effect of seasonal changes over time and the increment or decrement between band 1 and band 3 (Blue and Red), Chl-a mean concentrations for the influenced dates were concluded partially incorrect (e.g. 27th of August, 2010, and 23rd of

March, 2013). Furthermore, the specific algorithms chosen from the literature, they were not calibrated for the particular studied areas leading to an increase of the percentage of errors.

From the classification maps extracted from ENVI software package, TSI and turbidity showed a spatial correlation in locations which was assumed to present major differences between them. Moreover, it was also concluded that both algorithms performed equally well at Kourris dam. Concluding, both dams were classified as eutrophic.

5.2 General concluding remarks

Remote sensing techniques are the most easiest and economical way to detect and monitor water quality parameters in a systematic basis. The utilisation of specialised software has also revolutionised processing of satellite images by reducing the time needed for analysis. Their major disadvantage is that satellite's spatial and spectral resolution is still limited in contrast with in-situ advanced devices such as spectroradiometers. More specifically, satellites measure concentrations of Chl-a and turbidity as estimated mean values considering only the top surface of the examined water body. Therefore in-situ sampling is needed in order to validate estimated data retrieved from satellites.

In addition, remote sensing requires the involvement of numerous parameters such as evapotranspiration, detailed atmospheric conditions, and climatology and satellite sensor characteristics in order to represent environment's complex and unpredictable modelling system. Despite this, remote sensing is capable to provide an approximate estimation describing phenomena that in the past were not possible to be measured and predicted easily.

REFERENCES

Aggarwal, S. (n.d.). Principles of Remote Sensing. *Satellite Remote Sensing and GIS Applications in Agricultural Meteorology, pp.23-38.* Retrieved from http://www.wamis.org/agm/pubs/agm8/Paper-2.pdf

Augosto-Silva, P. B., Ogashawara, I., Barbosa, C. C. F., Carvalho, A. S. L., Jorge, S. F. D., Fornari, I. C. & Stech, L. J. (2014). Analysis of MERIS Reflectance Algorithms for Estimating Chlorophyll-a Concentration in a Brazilian Reservoir. *Remote Sensing, 6, 11689-11707*. doi:10.3390/rs61211689

Boronina, A., Renard, P. Balderer, W. & Christodoulides, A. (2003). Groundwater resources in the Kouris catchment (Cyprus): data analysis and numerical modelling. *Journal of Hydrology, 271, 130-149.* doi: 10.1016/S0022-1694(02)00322-0.

Carlson, E. R. (1977). *A trophic state index for lakes. Limnology and Oceanography, 22, 361-369*. Retrieved from http://link.springer.com/article/10.1065/espr2002.12.142

Centre of Remote Imaging, Sensing & Processing. (2001). *Analog and Digital Images.* Retrieved from http://www.crisp.nus.edu.sg/~research/tutorial/image.htm

Department of Meteorology Department of Metereology. (2016). Recent Weather Data. Retrieved from http://tinyurl.com/zvd3g6k

Dogliotti, A. I., Ruddick, K. G., Nechad, B., Doxaran, D. & Knaeps, E. (2015). A single algorithm to retrieve turbidity from remotely-sensed data in all coastal and estuarine waters. *Remote Sensing of Environment 156, 157-168.* doi: 10.1016/j.rse.2014.09.020

Finn, P. M., Reed, D. M. & Yamamoto, H. K. (n.d.). A Straight Forward Guide for Processing Radiance and Reflectance for EO-1 ALI, Landsat 5 TM, Landsat 7 ETM+, and ASTER. *United States Geological Survey.* Retrieved from http://tinyurl.com/jtffbzw

Food and Agriculture Organisation of the United Nations. (n.d.). *Chapter 4 – Remote Sensing as a data source*. Retrieved from http://tinyurl.com/zsxm7kk

Fuller, M. L. & Jodoin, S. R. (2016). Estimation of a Trophic State Index for Selected Inland Lakes in Michigan, 1999-2013 (Scientific Investigations Report 2016-5023). *U.S. Geological Survey*. doi: 10.3133/ sir20165023.

Geological Survey Department. (2016). *Geological Map*. Retrieved from http://www.moa.gov.cy/moa/gsd/gsd.nsf/dmlGeoMap_en/dmlGeoMap_en?OpenDocument

Gilerson, A. A., Gilerson, A. A., Zhou, J., Gurlin, D., Moses, W., Ioannou, I. & Ahmed, A. S. (2010). Algorithms for remote estimation of chlorophyll-a in coastal and inland waters using red and near infared bands. *Optical Society of America, 18(23),24.* doi:10.1364/OE.18.024109

Hadjimitsis, G. D., Hadjimitsis, G. M., Clayton, C. & Clarke, A. (2006). Determination of Turbidity in Kourris Dam in Cyprus Utilising Landsat TM Remotely Sensed Data. *Water Resources Management, 20, 449-465*. doi:10.1007/s11269-006-3089-y

Han, B., Loisel, H, Vantrepotte, V., Meriaux, X., Bryere, P., Ouillon, S, Dessailly, D., Xing, Q. & Zhu, J. (2016). Development of a Semi-Analytical Algorithm for the Retrieval of Suspended Particulate Matter from Remote Sensing over Clear to Very Turbid Water. *Remote Sensing, 8(3), 1-23*. doi:10.3390/rs8030211

Harris Geospatial Solutions. (2013). *Digital Number, Radiance and Reflectance.* Retrieved from http://tinyurl.com/jllv339

Huang, C., Zou, J., Li, Y., Yang, H., Shi, K., Li, J. Wang, Y., Chena, X. & Zheng, F. (2014). Assessment of NIR-red algorithms for observation of chlorophyll-a in highly turbid inland waters in China. *Journal of Photogrammetry and Remote Sensing, 93, 29-39.* doi: 10.1016/j.isprsjprs.2014.03.012

Jacobsen, K. (n.d.). Geometric Calibration of Space Remote Sensing Cameras for Efficient Processing. Retrieved from http://tinyurl.com/zu9avzn

Minnesota Pollution Control Agency. (2008). *Turbidity: Description, Impact on Water Quality, Sources, Measures – A General Overview.* Retrieved from https://www.pca.state.mn.us/sites/default/files/wq-iw3-21.pdf

Mousivad, A., Verhoef, W., Menenti, M. & Gorte, B. (2015). Modeling Top of the Atmosphere Radiance over Heterogeneous Non-Lambertian Rugged Terrain. *Remote Sensing, 7, 8019-8044.* doi:10.3390/rs70608019

Papoutsa, C. & Hadjimitsis, D. (2013). Remote Sensing for Water Quality Surveillance in Inland Waters: The Case Stuy of Asprokremmos Dam in Cyprus. *Remote Sensing of Environment: Integrated Approaches, 132-153.* http://tinyurl.com/jn9atyg

Papoutsa, C. (2015). *Integrated Use of Field Spectroscopy and Satellite Remote Sensing for Monitoring Water Quality in Case-2 (inland & coastal) Water Bodies* (Doctoral dissertation). Cyprus University of Technology, Faculty of Engineering and Technology, Lemesos, Cyprus.

Papoutsa, C. (2016, January). *Field Spectroscopy*. Unpublished intranet document, Cyprus University of Technology.

Papoutsa, C., Akylas, E. & Hadjimitsis, D. (2014). Trophic State Index deriviation through the remote sensing of Case-2 water bodies in the Mediterranean Region. *Central European Journal of Geosciences, 6(1), 67-78.* doi: 10.2478/s13533-012-0161-4

Papoutsa, C., Kounoudes, M. M., Toulios, M., Retalis, A., Kyrou, K. & Hadjimitsis, D. (2012). Monitoring turbidity in Asprokremmos dam in Cyprus using earth observation and smart buoy platform. *European Water, 38, 25-32.* Retrieved from http://ktisis.cut.ac.cy/jspui/handle/10488/8626

Papoutsa, C., Retalis, A., Toulios, L. & Hadjimitsis, D. (2014). Defining the Landsat TM/ETM+ and CHRIS/PROBA spectral regions in which turbidity can be retrieved in inland water bodies using field spectroscopy. *International Journal of Remote Sensing, 35(5), 1674-1692.* doi: 10.1080/01431161.2014.882029

Philpot, W. (2014). *Atmospheric Correction* (Lecture Notes). Retrieved from http://ceeserver.cee.cornell.edu/wdp2/cee6150/Lectures/DIP13_Atmospheric%20Correction.pdf

Potes, M., Costa, J. M. & Salgado, R. (2012). Satellite remote sensing of water turbidity in Alqueva reservoir and implications on lake modelling. *Hydrology and Earth System Sciences, 16, 1623-1633*. doi:10.5194/hess-16-1623-2012

Prasad, D. G. A. & Suddaraju. (2012). Carlson's Trophic State Index for the assessment of trophic status of two Lakes in Mandya district. *Advances in Applied Science Research, 3(5), 2992-2996.* Retrieved from http://tinyurl.com/jnwc67g

Rhode Island Department of Environmental Management - Office Water Resources. (2011). *Standard Operating Procedure for Secchi Disk Measurements SOP-WR-W-7.* Retrieved from http://www.dem.ri.gov/pubs/sops/wrw7.pdf.

Ritchie, C. J., Zimba, V. P. &. Everitt, H. J. (2003). Remote Sensing Techniques to Assess Water Quality. *Photogrammetric Engineering and Remote Sensing, 695-704.* doi:10.14358/PERS.69.6.695

Schaber-Schoor, G. (2010). *The European Water Framework Directive: Goals implementation in Baden-Wurttemberg*. Retrieved from http://tinyurl.com/jmuv6vw

Smith, D. G. & Hoover, M. (2000). Standardization of secchi disk measurements, including use of a viewer box. *Proceedings of the 2000 National Water Quality Monitoring Conference.* Retrieved from http://tinyurl.com/z28dpe3

Spectral Sciences, Incorporated. (2016). *About MODTRAN*. Retrieved from http://modtran.spectral.com/modtran_about

Stednick, J. D. & Hall, B. E. (n.d.). Applicability of trophic status indicators to Colorado plains reservoirs. Completion Report No. 195. *Colorado Water Resources Research Institute.* Retrieved from http://www.cwi.colostate.edu/publications/cr/195.pdf

Torbick, N., Hu, F., Zhang, J., Qi, J., Zhang, H. & Becker, B. (2008). Mapping Chlorophyll-a Concentrations in West Lake, China using Landsat 7 ETM+. *Journal of Great Lakes Research, 3, 559-565.* doi: 10.3394/0380-1330(2008)34[559:MCCIWL]2.0.CO;2

United States Geological Survey. (2016). *Frequently asked Questions about the Landsat Missions – What are the band designations for the Landsat satellites?*. Retrieved from http://landsat.usgs.gov/band_designations_landsat_satellites.php

United States Geological Survey. (2016). *Landsat 8 (L8) Data Users Handbook – Section 5*. Retrieved from http://landsat.usgs.gov/l8handbook_section5.php

United States Geological Survey. (n.d.). *Landsat Spectral Bands*. Retrieved from http://igett.delmar.edu/Resources/Remote%20Sensing%20Technology%20Training/Landsat_bands-sm.pdf

Usali, N. & Ismail, H. M. (2010). Use of Remote Sensing and GIS in Monitoring Water Quality. *Journal of Sustainable Development, 3(3), 228-238*. doi:10.5539/jsd.v3n3p228

Water Development Department. (2002). *Use and conservation of water in Cyprus.* Retrieved from http://tinyurl.com/jmc3l4q

Yang, Z. & Anderson, Y. (2016). Estimating Chlorophyll-A Concentration in a Freshwater Lake Using Landsat 8 Imagery. *Journal of Environment and Earth Science, 6(4), 134-142.* Retrieved from http://tinyurl.com/j5b5mba